CHAPTER 3

PROTOTYPE DESIGN, CALIBRATION, METHODOLOGY AND PERFORMANCE ANALYSIS

3.1 Introduction:

Tissue phantoms must possess the scattering and absorption phenomenon similar to that of living human tissues in all respect along with their wavelength detection criteria. Tissue phantom refractive index properties are required to match with that of living tissue refractive index. The functional and tissue mimicking properties must be steady enough and not to be influenced by temperatures, humidity, photo bleaching and other environmental conditions. The tissue phantoms with low cost of production, easy processing, greater stability, high optical tissue resemblance, and logistics friendly are popular now days. The above-mentioned features are needed in tissue phantom to model blood glucose properties of human body, and it is required for the design and development of noninvasive bio sensing of blood glucose in human body. The major difficulty in the development of a clinical application of optical noninvasive blood glucose sensors is associated with the very low signal produced by glucose molecules [Tuchin *et al.* (2011)].

A realistic noninvasive blood glucose sensing tissue phantom is required to have the following features:

(i) It should be able to model the physiological feature that includes: geometry and optical properties of the living tissue form light transport phenomenon point of view.

(ii) Tissue phantom composition must be stable for providing better chemical stability and spectroscopic properties.

(iii) Sample composition must provide reproducible results typically for radiation transport measurement.

(iv) The physical factors of the phantom sample should be temporarily stable for evaporation, diffusion, and aging it must be independent of environmental influence.

(v) The construction of inhomogeneous samples may be prepared by stacking phantom slabs or by elaborate molding techniques using tissue phantom compositions.

(vi) Easy, safe, handy and faster sample preparation procedures.

3.1.1 Role of Intralipid^{TM} based tissue phantom:

Present work contains the information about tissue mimicking phantom, preparation of Intralipid^{TM} based tissue phantom and utilization of Intralipid^{TM}

phantom for developing our principle Modulated Ultrasound and Infrared (MUS-IR) light technique by performing the *in-vitro* investigations on different biological samples.

3.1.2 Tissue mimicking phantom:

The utilization of optical constituents, which resemble the optical characteristics of biological tissue, is broadly applied in the field of biomedical for studying the light transport characteristics. These optical constituents are generally termed as tissue mimicking 'Phantoms'. The necessity of tissue mimicking phantom for the development of optical technique and instrumentation are constantly rising for medical application purposes. The use of tissue mimicking phantoms in the field of biomedical optics research area are well described by [Pogue *et al.* (2006)]. To construct the phantom medium the absorbing and scattering particles are added as the base substances. The base substance may be present in the form of liquid or solid. Some liquid phantoms generally used are aqueous based lipid, oil, milk and fat. The solid phantom used as Titanium dioxide scatterers inserted in polystyrene resin. Intralipid^{TM} phantom medium typically used in this experimental work for evaluating the functioning of our designed prototype [Cletus (2010)].

Intralipid^{TM} generally appears as milky white in colour. It is used for feeding the fat deficient weak persons for energy and fat. For making the similarity in optical scattering characteristics of different biological tissue, the Intralipid^{TM} phantom may be diluted according to the need. The Intralipid^{TM} suspension has been made using (i) soybean oil, (ii) egg lecithin, (iii) glycerin and (iv) water. The encapsulation of soybean oil by a monolayer membrane of lecithin is responsible for the scattering property of Intralipid^{TM}. The name of Intralipid^{TM} is derived from its "inside the lipid" characteristics [Cletus (2010)].

To mimic the properties of human or animal tissues, the use of tissue mimicking objects plays a significant role. They are well calibrated for routine system evaluation and standardization. For all reasons, good quality phantoms is essential for research purposes. To match the optical characteristics of tissues with phantom preparations, it depends on understanding of key physical and chemical properties of the tissues involved. In the present work the finger phantom with optically similar to finger has been prepared as proposed in references [Burmeister *et al.* (1998); Van Staveren *et al.* (1991)].

3.1.3 Preparation of Intralipid^{TM} based tissue phantom:

Intralipid^{TM} is an aqueous suspension of lipid droplets that is sterile and used as phantom for mimicking tissue optical properties. Available as Intralipid^{TM} 10% and Intralipid^{TM} 20% (10% lipid indicates 10 g of lipid per 100 ml of suspension). The Table 3.1 represents the constituents of Intralipid^{TM} 10% in a 500 ml total volume. The figure 3.1 represents the preparation of Intralipid^{TM} tissue phantom for our *in-vitro* experimental purposes.

Table 3.1: Different constituents of 10% Intralipid^{TM} suspension [Flock *et al.* (1992); Van Staveren *et al.* (1991)].

Constituents	Unit in (g)	Unit in (ml)
Soybean oil	50 g	53.94 ml
Lecithin	06 g	5.82 ml
Glycerin	11.25 g	8.92 ml
Water	430.5 g	431.33 ml
Total	497.75 g	500 ml

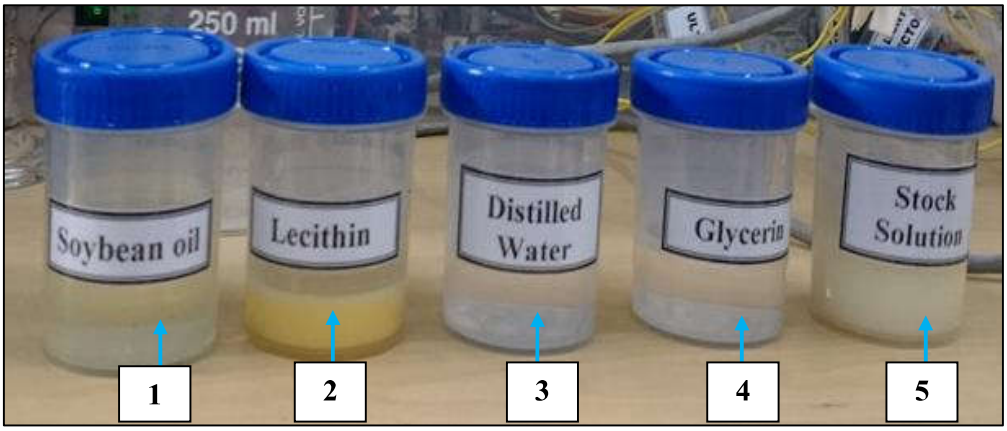

Figure 3.1: Preparation of Intralipid^{TM} tissue phantom and its different constituents; (1) Soybean, (2) Lecithin, (3) Distilled water, (4) Glycerin, (5) Finally stock solution utilized for *in-vitro* investigation.

Variation in optical property of Intralipid^{TM} occurs from 10% Intralipid^{TM}, 20% Intralipid^{TM} and 30% Intralipid^{TM}. Hence, standardization and calibration of the Intralipid^{TM} sample before experimental work is essential. Optical characteristics of

Intralipid^{TM} have been stated by various groups using different photon migration techniques over different wavelength spectral regions [Flock *et al.* (1992); Staveren *et al.* (1991)].

3.2 Principle of modulated ultrasound and infrared light-based prototype design for glucose concentration measurement in *in-vitro* biological samples:

Zhu *et al.* (2013) and Zhu *et al.* (2010) introduced a methodology of using ultrasound modulated optical technique for blood glucose-concentration determinations. Their *in-vitro* studies were based upon the measurement of ultrasonic modulation depth through ultrasound modulated scattered light. They introduced the application of ultrasound with light modulation techniques [Zhu *et al.* (2013); Zhu *et al.* (2010)]. However, in this present work, the modulated ultrasound exhibits vibrations inside the *in-vitro* phantom samples and the infrared light measures the glucose molecule specific vibrations for glucose concentration measurement [Srivastava *et al.* (2016)].

When ultrasonic waves with amplitude modulation characteristics propagates through the *in-vitro* phantom samples, the molecules present within that medium experiences vibrations due to the impact of pressure exhibited by the amplitude modulating ultrasonic waves. The inherent characteristics of molecules existing within that *in-vitro* sample medium effect the compressibility factor of the medium. The physical properties of the molecules existing within that *in-vitro* medium exhibit the vital role. The degree of influence over larger molecules are larger and vice-versa [Radel *et al.* (2010); Ter Haar *et al.* (1978)].

Henceforth, the vibration generated in that *in-vitro* sample medium depends on (a) its three dimensional organizations, (b) inherent characteristics of the *in-vitro* sample molecules, (c) nature and characteristics of the amplitude modulated ultrasonic waves [Coakley (1997); King (1934)].

The ultrasonic wave possesses amplitude maximum and minimum values two times over the space of one unit wavelength. Inside the ultrasound-propagating segment, the molecules attain area definite ultrasonic potential energy owin to their existence in that particular domain. The suspended molecules initiate to travel and gather adjacently to the area of low ultrasonic potential energy. Generally, these areas are located nearby to the pressure nodes, spaced from each other by half a wavelength distances [Petersson *et al.* (2004); Yosioka *et al.* (1955)].

Afterwards, when the molecular physical characteristics is lesser than the wavelength of the transmitting ultrasound within the *in-vitro* phantom samples, the foremost radiation force (F_r) applied over the molecular volume (V_c), located by space (z) starting from the node of pressure is measured from the molecular ultrasonic potential energy based gradient values and scientifically represented as:

$$F_r = -\left[\frac{\pi p_o^2 V_c \beta_w}{(2\lambda)}\right].\phi(\beta,\rho).\sin(4\pi z/\lambda) \qquad \text{Equation (3.1)}$$

In this present work, the (P_o) signifies ultrasonic peak amplitude. (λ) stands for wavelength of ultrasound in that *in-vitro* sample medium. The compressibility of the medium have been denoted as (β_w), and scientifically represented [Radel *et al.* (2010); Coakley (1997)] as:

$$\phi(\beta,\rho) = [\frac{5_{\rho_c} - 2_{\rho_w}}{2_{\rho_c} + \rho_w} - \left(\frac{\beta_c}{\beta_w}\right)] \qquad \text{Equation (3.2)}$$

Here, the molecular compressibility have been denoted as (β_c). Further, the symbols (ρ_c) and (ρ_w) represents molecular density and suspending segment density respectively [Radel *et al.* (2010); Coakley (1997)].

To quantify the specific absorption (A) characteristics of the glucose molecules at a particular light wave number (v), the famous Lambert-Beer law has been introduced and scientifically represented as:

$$A(v) = -\log I(v)/I_0(v) \qquad \text{Equation (3.3)}$$

Herein, the (I_o) stands for the surrounding area light intensity and (I) signifies the particular light intensity at specific wave number (v) of the *in-vitro* sample measurements [Radel *et al.* (2010); Coakley (1997)]. Henceforth, we attain the advantage of beam formation at the specific frequency of ultrasound for focusing the radiation force of energy towards the *in-vitro* optical phantom sample mediums. This generates vibration characteristics at lower frequencies, for which the displacements are adequate enough for measurement with the help of infrared red light based techniques accordingly [Urban *et al.* (2010); Urban *et al.* (2006]. In this present work, the entire observed signal undergoes signal analysis through the signal processing

toolbox of MATLAB. The peak amplitude in the FFT (Fast Fourier Transform) domain were monitored here to extract glucose concentration based embedded information from the observed signals as acquired from the *in-vitro* samples.

3.2.1 Descriptions of the fabricated prototype:

The figure 3.2 represents the block diagram description of our developed technique based prototype Modulated Ultrasound and Infrared Red (MUS-IR) unit for estimating the glucose concentrations in the different biological sample mixed Intralipid^{TM} phantom based *in-vitro* investigations.

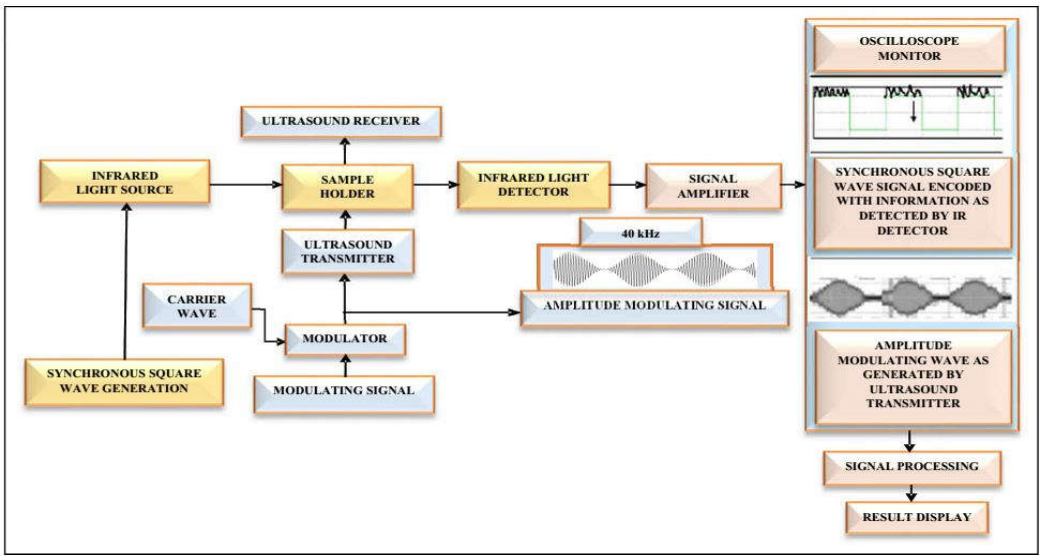

Figure 3.2: Block diagram of our *in-vitro* technique based prototype (MUS-IR) unit.

Our prototype-based technique utilizes modulated ultrasound and infrared light based technique for *in-vitro* measurement of glucose concentration levels. The modulating signal unit provides modulating sine wave signals and the carrier wave unit provides carrier wave signals. Both these modulating and carrier wave signals are used as an input to the modulator unit. The modulator unit produces amplitude modulated sine wave signals to the ultrasound transmitter unit. The Ultra-Sound-Transmitter (UST) unit produces ultrasonic amplitude modulated sine waves to the sample holder unit.

The amplitude modulated ultrasonic waves excites the sample, as a result the different constituent molecules vibrates at their specific response frequency

depending upon their size, shape, weight and properties of the medium in which they are present [Radel *et al.* (2010); Coakley (1997)].

The Ultra-Sound-Receiver (USR) unit used here to cross checks the pattern of amplitude-modulated signal waves as produces by ultrasound transmitter unit (shown in the oscilloscope monitor block in figure 3.2 respectively). The synchronous square wave generations are provided to the Infrared light source unit, to produce square wave pulses to the sample holder unit. Further, the specific vibrations produced due to amplitude modulated ultrasonic waves are detected by using the infrared light detector unit. The amplified output response signal is in the form of synchronous square wave signals as shown in the oscilloscope monitor block of figure 3.2, which carries encoded information about the concentration of different constituent molecules. This modulated light response signal, collected using Infrared light detector are suitably processed to extract the information about the glucose concentration and then the display unit shows the results [Srivastava *et al.* (2016); Chowdhury (2015)].

3.2.2 Prototype fabrication (MUS-IR unit):

The descriptions about ultrasonic transducers (UST and USR units) and light wavelength selection criterion have been given in this chapter. Subsequently, this chapter contains illustrations of the fabricated prototype (MUS-IR unit). For validating the *in-vitro* test results, this chapter incorporates the application of Error Grid analysis (Clarke and Parkes) and statistical analysis.

3.2.3 Selection of ultrasonic operating frequency:

Ultrasonic transducers have found various applications in house hold accessories, therapeutic fields, commercial enterprises, and oceanography. One such essential part of the hardware is the 40 kHz piezoelectric based ultrasonic transducers. This kind of piezo sensor has been widely used in remote controls, hostile to robbery gadgets, auto stopping sensors, and so forth [Se-yuen (2003); Greenslade (1994)]. Radel *et al.* (2010) used ultrasonic control strategies to enhance affectability of infrared spectroscopy for chemical analytical characterization. The incorporation of both these methodologies has produced the new idea for use in suspension's chemical analysis. Restricted accumulation of particles by utilization of ultrasound helps the determination of molecule particular infrared signatures of the suspending particles and medium correspondingly. Changing the frequency of ultrasonic standing waves controls the position of the molecules in the optically responsive region in the infrared

spectroscopy. They have used this way to evaluate polystyrene molecule concentrations in methanol suspension and expressed significant results.

Additionally, the Table 3.2 represents biomedical applications of 40 kHz or lower frequencies of ultrasonic transducer systems are as per the following:

Table 3.2: Significant literature on biomedical research application of 20-40 kHz for selection of ultrasound frequency.

Explorations by different researchers	**Ultrasound frequency**	**Utilized in different applications**
Suchkova *et al.* (1998)	40 kHz	Applied for tissue penetration, fibrinolysis and warming purpose.
Birnbaum *et al.* (1998)	37 kHz	In-vivo coagulate disintegration.
Suchkova *et al.* (2000)	40 kHz	Enhances perfusion of tissue and thrombolysis.
Lee *et al.* (2005)	20 to 40 kHz	Penetrates rat skin for blood glucose monitoring.
Voigt *et al.* (2011)	20 to 40 kHz	Wound healing therapy.

Fairly moved by this aforementioned methodology, in our precise *in-vitro* glucose estimation purpose, we have used amplitude modulation with focal ultrasonic frequency of 40 kHz to start essential excitation in the specific estimation in Intralipid^{TM} based tissue phantom. Additionally, (i) Easy accessibility, (ii) Clinically safe for biological samples and tolerable (iii) Less warming in the medium, (iv) High penetration in tissue like medium, and (v) Low cost of 40 kHz ultrasonic transducers have inspired us for its vital selection.

3.2.4 Selection of light wavelength:

The glucose molecule-absorption bands superimpose with the molecules of water absorption bands. The circumstance turns out to be more complex because of the differed nature of the human blood characteristics and its biological tissues optical characteristics [So *et al.* (2012)].

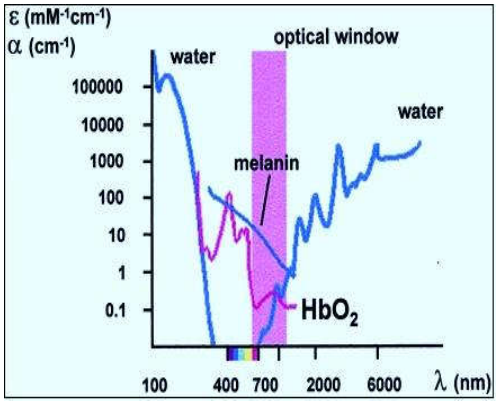

Figure 3.3: Absorption profile of main intracellular absorbers [Konig (2000)].

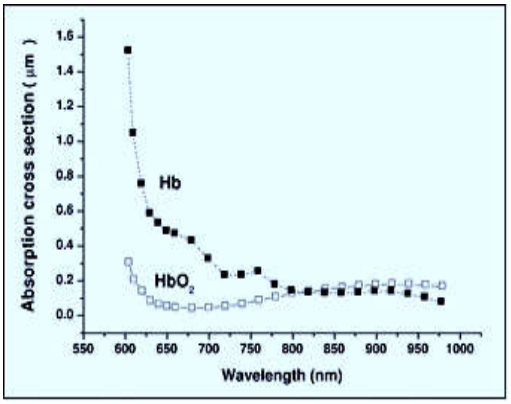

Figure 3.4: Absorption pattern of oxyhemoglobin and reduced hemoglobin from 550 nm to 1000 nm respectively [Tuchin (2009); Mendelson (1992); Assendelft (1970)].

Henceforth, wavelength selection must be particular and glucose molecule oriented [Konig (2000); Tenhunen *et al.* (1998)]. The figure 3.3 illustrates the absorption profile of main intracellular absorbers. It signifies the molecular extinction coefficients (ε) of skin colour containing melanin and hemoglobin in oxygenated structure. It also signifies the absorption coefficient (α) of water correspondingly (as shown in figure 3.3 the optical window). The insufficiency of the efficient one-photon absorbers causes the natural cells and tissues to be optically visible in the wavelength (λ) range from 700 nm to 1100 nm correspondingly. Further, the figure 3.4 signifies that oxyhemoglobin (HbO_2) and reduced hemoglobin absorption properties are relatively less responsive in Red and NIR wavelength ranges correspondingly. Therefore, the spectral band extending from 700 nm to 1100 nm is commonly termed as "Optical Window" of the living natural tissues [Kulkarni *et al.* (2010); Konig (2000)].

Blood-oxygenations concentrations change the blood optical absorption characteristics [Kulkarni *et al.* (2010); Tuchin (2009)]. The figure 3.4 illustrates that the absorption spectrum range of oxyhemoglobin and deoxyhemoglobin is relatively low between the spectral wavelength range from 900 nm to 1000 nm correspondingly. Consequently, blood glucose estimation within this region (900 nm to 1000 nm) provides less intervention from other sources of errors [Tuchin (2009); Mendelson (1992)].

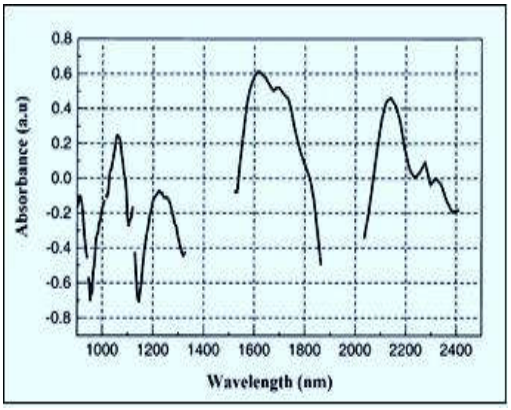

Figure 3.5: Absorption characteristics of glucose dissolved in water within the NIR and IR spectral region [Tenhunen *et al.* (1998)].

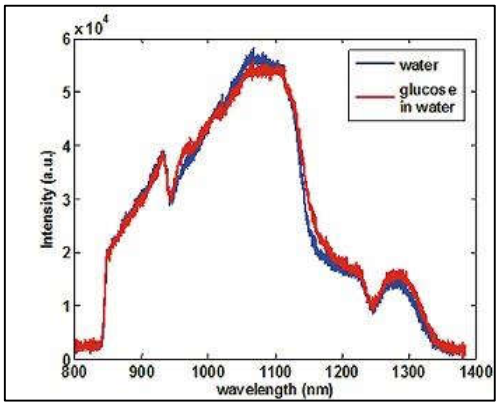

Figure 3.6: Absorption profile of water and glucose in water at 800 nm to 1400 nm regions [Beckers (2013)].

Table 3.3: Absorption features dependent stretch and vibration patterns of the glucose molecule [Khalil (1999)].

Significant Wavelengths for Glucose Molecule Determination							
Wavelength (nm)	939	1126	1408	1536	1688	2261	2326
Possible Stretch and Vibration	3*v*OH	3*v*CH	2*v*OH	*v*OH + *v*CH	2*v*CH	*v*CH + *v*CCH, OCH	*v*CH + *v*CCH, OCH
Description	Second OH overtone band	Second harmonic CH overtone band	First OH overtone band	OH and CH combination band	CH overtone band	Combination of a CH stretch and a CCH,OCH deformation	

The figure 3.5 and Table 3.3 represents glucose molecules absorption peaks in the wavelength ranges at 939 nm (near 940 nm), 1126 nm,1408 nm, 1536 nm, 1688 nm, 2261 nm, and 2326 nm respectively [Khalil (1999); Tenhunen *et al.* (1998)]. Correspondingly, the figure 3.6 represents that the glucose molecules shows the absorption peaks close to 940 nm spectral range where water appears to share same profile, however for most of the time its concentration are processed as steady background signals [Beckers (2013)]. Furthermore, for self-confirmation here, we investigate the prepared 10% glucose (dextrose)-distill water solution and observed the absorption peak of the glucose molecule in the spectral range from 300 nm to

1050 nm by utilizing Mini-spectrometer (AvaSpec-ULS2048-USB2-VA-50) of Avantes Inc., USA.

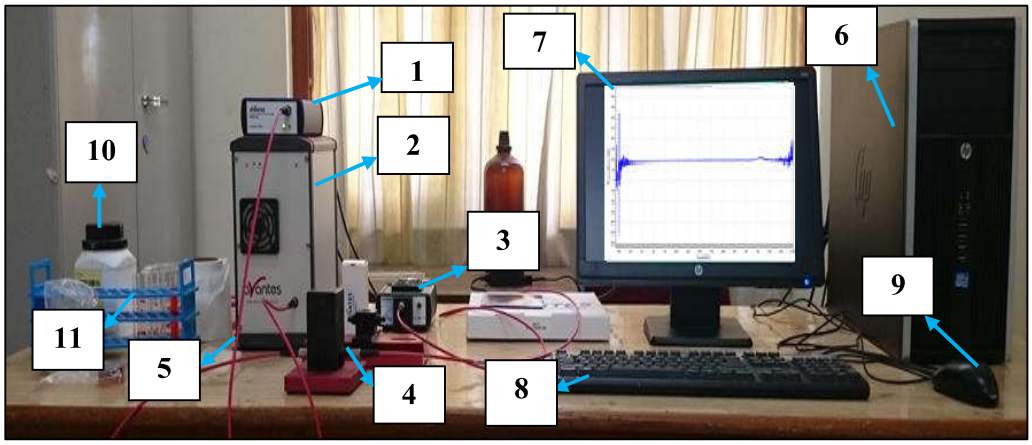

Figure 3.7: Mini-spectrometer of Avantes Inc., USA;
1. Ultraviolet-Visible range spectrometer, 2. Infrared range Spectrometer, 3. Light source, 4. Sample holder with cover and stand, 5. Optical fiber, 6. Central processing unit, 7. Spectral reading program in computer display, 8. Keyboard, 9. Computer mouse, 10. Dextrose powder bottle, 11. Test tube stand.

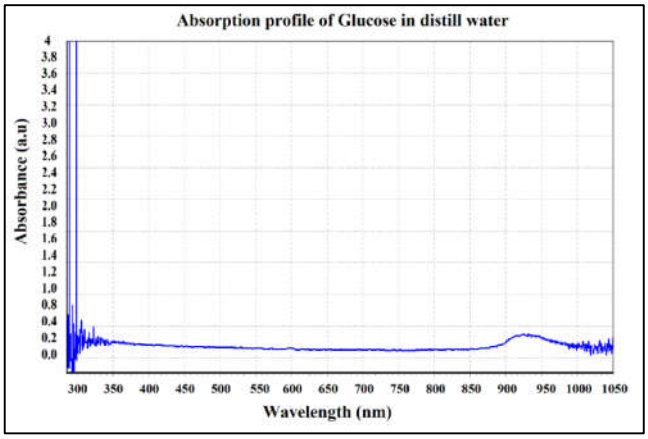

Figure 3.8: Absorption characteristics of 10% Dextrose (glucose)-distill water between 300 nm to 1050 nm respectively.

The figure 3.7 represents the complete instrumental system of Mini-spectrometer of Avantes Inc., USA used in this present experimental work. The figure 3.8 illustrates the absorption profile of 2 ml (10%) glucose in distill water solution

and also shows the absorption profile of glucose molecule very close to 940 nm wavelength.

Consequently, in view of wavelength such as 940 nm where oxyhemoglobin, decreased hemoglobin, water and additional main intracellular absorbers shows low absorption profiles and fine absorption profile from glucose molecules will be ideal to prevent any sort of specific noise obstructions [Kulkarni *et al.* (2010); Tuchin (2009)]. Further, Table 3.4 illustrates the different research specialists have used 940 nm for noninvasive glucose estimation methods. Some research specialists in this field utilized 940 nm IR LED are provided as follows:

Table 3.4: Researchers using 940 nm wavelength for measuring glucose non-invasively.

Explorations by different researchers	**940 nm wavelength utilized for non-invasive glucose measurement used in different approaches**
Yeh *et al.* (2003)	Used 935 nm (near to 940 nm) for glucose concentration effects over skin thermo optical responses.
Cho *et al.* (2004)	Used 950 nm (extremely close to 940 nm) as metabolic heat conformation methods.
Iiya Fine (2009)	Investigated as the reference LED wavelength.
Tirtariyadi (2009)	For developing optical glucometer by NIR bio sensing application.
Kulkarni *et al.* (2010)	905 nm laser diode (close to 940 nm) applied in Photo Acoustic Spectroscopy.
Vashist *et al.* (2012)	Used Near Infrared wavelength for Sugar Tracking.
Bin *et al.* (2013)	Applied two wavelengths 940 nm and 950 nm reported raise in linear voltage yield with rise in glucose concentration.
Pandey *et al.* (2013)	Connection between real blood glucose levels and the DSO (Digital Storage Oscilloscopes) based yield voltages above more than eight patients correspondingly.
Yadav *et al.* (2014)	Designed Near Infrared LED supported noninvasive glucose biosensor.

The outcomes are reliable and demonstrated the potentiality of the 940 nm Near Infrared wavelength in estimating blood glucose levels through the noninvasive systems. Taking into the occurrences of the tissue optical window, the wavelength of 940 nm has been considered here for the experimental work.

3.2.5 *In-vitro* experimentations:

In this present work, the *in-vitro* investigation assesses the glucose specificity and sensitivity perspectives. The specificity indicates to the specific light wavelength where glucose shows most optimum absorption-peak properties. Essentially, the sensitivity indicates to the capability of the specific light wavelength to react in respect with the efficient alterations in the glucose concentration levels.

3.2.5.1 Specificity analysis of glucose molecule:

To ascertain the optimum wavelength specificity of glucose in distill water within of 900 nm to 980 nm wavelength region, during experimentation the preparation of stock solution of 2000 mg dextrose (glucose) per 10 ml of distill water for experimental propose was done.

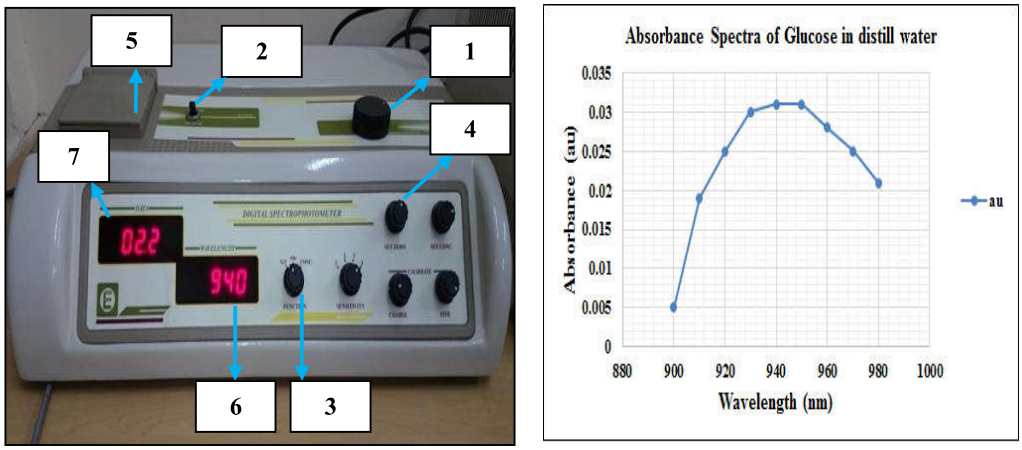

(a) **(b)**

Figure 3.9 (a): Digital spectrophotometer of M.S Electronics Pvt. Ltd. (India); 1. Wavelength selection knob, 2. Wavelength range (UV or Visible) selection panel, 3. Absorption and Transmittance selection modes, 4. Coarse adjustment knobs, 5. Sample holder with cover lids, 6. Wavelength display, 7. Result display **(b):** Absorption spectra of glucose in distill water in the range between 900 nm to 980 nm.

From the stock solution concentration in (weight/volume), the 2 ml of glucose in distill water solution has been pipette out, and poured inside the cuvette. The figure 3.9 (a) represents the Digital Spectrometer Model 305 of M.S. Electronics Pvt. Ltd. (India) that is utilized as a part of this present work to evaluate Absorbance (au = arbitrary unit) of glucose mixed up in distill water solution. The figure 3.9 (b) represents the absorption spectra of the glucose mixed in distill water and also shows that within Near Infrared spectral region of 900 nm to 980 nm, at 940 nm optimum absorption peak is observed.

Further, from Table 3.3, it can be represented that glucose molecule shows absorption peak properties at 939 nm (near to 940nm) because of possible stretch and vibration of the second OH overtone band [Khalil (1999)] in their molecular structure.

3.2.5.2 Sensitivity analysis of glucose molecule at 940 nm:

Different concentration (weight/volume) of dextrose is dissolved in distill water solution like 2000 mg/10 ml, 4000 mg/10 ml and 6000 mg/10 ml correspondingly. The above-mentioned solutions are prepared and utilized for determining the sensitivity of various glucose concentration at 940 nm wavelength.

For the glucose sensitivity, evaluation at 940 nm wavelength, the data from these 03 prepared sample concentration (weight/volume) solution has been represented in Table 3.5.

Table 3.5: Sensitivity analysis of glucose molecule at 940 nm.

Wavelength (nm)	2ml from the prepared sample solutions (w/v)	Absorbance (au)	Concentration (ppm)
940	2000 mg/10ml	0.029	065
	4000 mg/10ml	0.040	108
	6000 mg/10ml	0.062	146

The yield data in Absorbance (arbitrary unit = au) and Concentration (parts per million = ppm) represents that 940 nm wavelength has been sensitive in identifying particular alterations in glucose concentration (weight/volume) in the sample solution.

Henceforth, different factors like "Optical Window" range (700-1100) nm, typical peak pattern for the glucose molecule at 940 nm, acceptable specificity and sensitivity for glucose molecule at 940 nm, inexpensive and simple commercial accessibility, various literature surveys as documented above; preferring 940 nm for

in-vitro blood glucose estimation firmly impacted us for this specific wavelength application in our study.

3.2.6 Amplitude modulation generation:

In this present experimentation, the generation of amplitude modulation has been utilized in our MUS-IR unit. The figure 3.10 shows the generated amplitude modulated signal waveform pattern exhibited on the screen of DSO (Digital Storage Oscilloscope - Nvis 102 CT Digital Storage Oscilloscope of 25 MHz, 50MSa/s) based upon voltage and current variations in the time domain.

Table 3.6: Amplitude modulated signal characteristics.

Characteristics of amplitude modulated signal parameters	
CH1	5.00 V
Frequency (f)	40.38 kHz
V_{pp}	19.98 V
V_{rms}	5.78 V
+Dut	50.00%
-Dut	50.00%
+wid	11.98 µs
-wid	11.98 µs

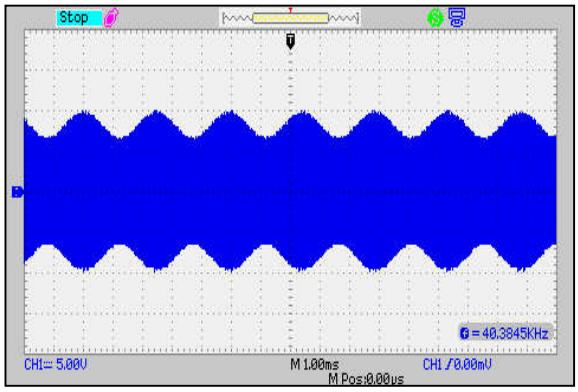

Figure 3.10: Amplitude modulated signal waveform.

The figure 3.10 and Table 3.6 shows the characteristics of amplitude modulated signal waveform as utilized in our MUS-IR unit. The produced signal waveform parameters in view of current and voltage variations for time domain as assessed by the DSO unit are indicated in Table 3.6 respectively. The CH1 (Channel 1 of DSO) has been chosen for this signal investigation. The frequency (f) of the Amplitude-Modulated (AM) signal has been 40.38 kHz. The V_{pp} and V_{rms} assessed values are 19.98 V and 5.78 V respectively. Its +duty and -duty cycles has been 50.00% and 50.00% respectively, their +width and -width has been 11.98 µs and 11.98 µs correspondingly.

Moreover, this signal act as an input to the Ultrasound Transmitter Unit to produce amplitude modulated ultrasonic signal waves inside the *in-vitro* samples to produce desired vibrations.

3.2.7 Ultra Sound Transmitter (UST) and Ultra Sound Receiver (USR) units:

In this present work, we have chosen Ultrasound Transmitter (UST) and Ultrasound Receiver (USR) of 40 kHz central frequency. The 40 kHz ultrasonic frequency is physiological safe for its application over biological samples [Se-yuen (2003)]. The characteristics and benefits of UST and USR units as per the manufacturer are as follows:

The ultrasound transmitter and ultrasound receiver transducer works at the central frequency of 40±1.0 kHz correspondingly. Commercially, both of it is available in coordinated couples with white or black net in aluminum casings. Transmitter can endure input voltage of 20 V_{rms} optimum and provides sound pressure level of 110±5 dB (approximately) at 10 V and 30 cm correspondingly. It has been reported that same system can be used as the Transmitter or the Receiver. Nevertheless, Transmitter (T) and Receiver (R) units have been illustrated with "T" and "R" behind their respective aluminum casings. The Receiver have the total mesh dimension of 7.5 m and its successful detecting zone is around 20 mm^2 correspondingly. Thus, the minimal power required for signal generation is $\frac{1}{2}V_{input}.I_{input} \approx 100\,mW$ correspondingly. The amplitude-modulated waves as produced from the particular modulator unit provides signal input to the UST unit. Hence, the UST utilitarian unit produces yield signal as ultrasonic amplitude modulated waves towards the sample holder unit. The figure 3.11 represents the diagram of this phenomenon.

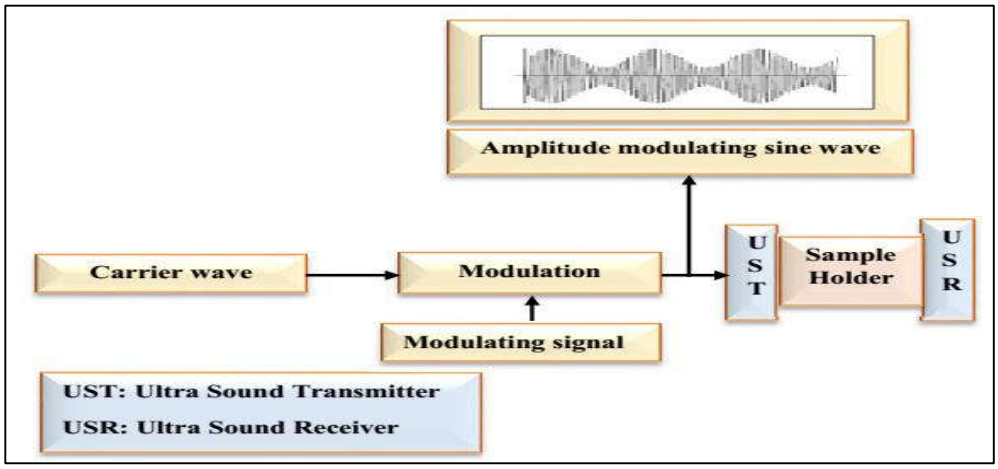

Figure 3.11: Amplitude modulated waveform characteristics as provided to the sample holder.

Table 3.7: Waveform characteristics as generated by the USR unit.

Characteristics of waveform of ultrasound receiver	
CH1	5.00 V
Frequency (f)	40.38 kHz
V_{pp}	9.80 V
V_{rms}	2.60 V
+Dut	50.00%
-Dut	50.00%
+wid	34.00 µs
-wid	34.00 µs

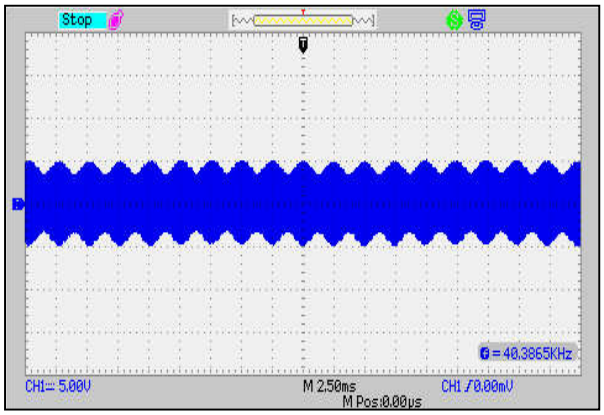

Figure 3.12: The output waveform pattern from the USR unit as recorded by DSO.

The figure 3.12 and Table 3.7 represents the yield waveform figure and its characteristics as assessed from the USR unit at resonance by the DSO. It shows in this present work, the CH1 (Channel 1 of DSO) has been chosen for this signal analysis. The frequency (f) of the yield waveform signal has been 40.38 kHz. The V_{pp} and V_{rms} assessed values are 9.80 V and 2.60 V respectively. Its +duty and -duty cycles has been 50.00% and 50.00% respectively. Moreover, their +width and -width has been 34.00 µs and 34.00 µs correspondingly. In this present work, the USR unit monitors the amplitude modulation working quality of ultrasonic waves produced from the UST unit towards the sample holder unit.

3.2.8 Sample holder unit:

Sample holder upholds the sample tube in exact geometrical position needed for precise ultrasonic wave propagation and Infrared light transmissions respectively.

Figure 3.13: Sample holder of our *in-vitro* technique based prototype unit.

The sample holder in figure 3.13 assists in stable positioning of Ultrasonic and Infrared light units, and for the sample tube positioning during signal obtaining procedures. Further, it reduces the undesirable errors such as wrong positioning and background light interferences.

3.2.9 Synchronous square wave production:

In this experimental work, we have chosen the function generator (3 MHz, HM-5030-4) of Scientific Pvt. Ltd (India) for the generation of square wave. This unit provides an input signal to operate the IR LED of 940 nm. To coordinate along with the heart cycle based pulsatile movement of the blood flow, the use of the square wave is a fundamental and essential [Tuchin (2009)]. The figure 3.14 and Table 3.8 represents the square wave input signal and its characteristics as assessed by the DSO.

Table 3.8: Square wave signal characteristics.

Characteristics of square wave signal	
CH1	500 mV
Frequency (f)	406.04 Hz
V_{pp}	1.19 V
V_{rms}	821.0 mV
+Dut	50.00%
-Dut	49.00%
+wid	1.25 ms
-wid	1.23 ms

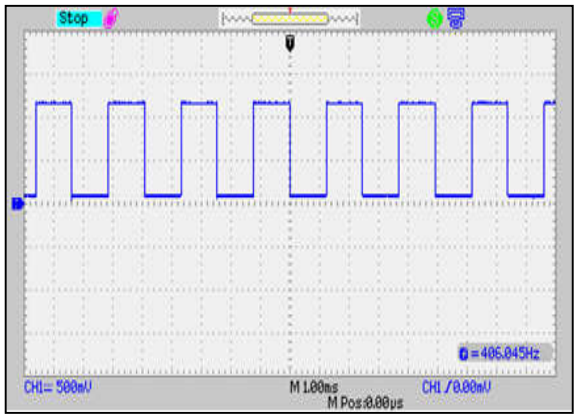

Figure 3.14: Square wave signal.

The Table 3.8 shows in this experimental work, the CH1 (Channel 1 of DSO) has been chosen for this signal examination. The frequency (f) of the square wave signal has been 406.04 Hz. The V_{pp} and V_{rms} assessed values are 1.19 V and 821.0 mV respectively. Their +duty and -duty cycles has been 50.00% and 49.00% respectively. Moreover, their +width and -width has been 1.25 ms and 1.23 ms respectively.

3.2.10 Infrared light source:

In this experimental work, we have used the 940 nm Infrared Light Emitting Diode (B5B-940-8) of Roithner-Laser-Technik Vienna, Austria, for treating *in-vitro* Intralipid^{TM} phantom mixed biological samples.

3.2.11 940 nm LED wavelength confirmation:

Infrared Light Emitting Diode (B5B-940-8) of Roithner-Laser-Technik-GmbH that has been cross examined for conforming their typical optimum spectral strength by using Mini-IR spectrometer (AvaSpec-ULS2048-USB2-VA-50) of Avantes Inc. USA.

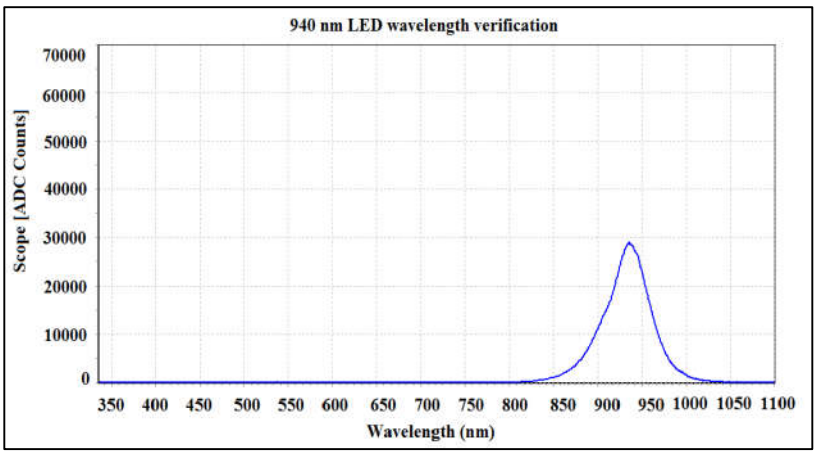

Figure 3.15: Maximum spectral intensity distribution of the IR LED used in our prototype unit.

The figure 3.15 demonstrates the ideal quality spectral strength close to 940 nm that fulfills the crucial necessity for our *in-vitro* investigation.

3.2.12 Infrared (IR) detector:

In this experimental work, we have used EPD-1300-5.3; InGaAs specific photodiode of Roithner-Laser-Technik, Vienna, Austria, for acquiring transmitted light from the infrared light (940 nm) used in *in-vitro* samples for estimating glucose levels. This photodiode is ideal for recognition of pulsed light with sensitivity beginning from 800 nm to 1750 nm.

3.2.13 Unit for signal processing:

In this experimental work, the entire observed signal undergoes signal analysis through the signal processing toolbox of MATLAB. The peak amplitude in the FFT (Fast Fourier Transform) domain were monitored here to extract glucose concentration based embedded information from the observed signals as acquired from in-*vitro* samples.

3.2.14 Result display:

This portion of the prototype unit represents the Predicted Blood Glucose Level in mg/dl for *in-vitro* samples.

3.3 *In-vitro* experiment:

With a specific goal to establish a technique for blood glucose estimation at first, (i) *in-vitro* experiments utilizing glucose solution in aqueous form and (ii) *in-vitro* optical tissue phantom based analyses are extremely significant. Optical phantoms be similar to tissue optical characteristics, in which different elementary concepts, scientific ideas are investigated [Amir *et al.* (2007); Kohl *et al.* (1995)].

3.3.1 *In-vitro* investigation utilizing glucose in distill water:

Our underlying step contains glucose solution based *in-vitro* studies to investigate the estimation principle of our modulated ultrasound and infrared light based technique. The glucose concentration range is selected from 0 mg/dl to 1500 mg/dl. The preparation of stock solution of different ratio of dextrose anhydrous, purified powder from (Merck specialties private limited) like 0 to 1500 mg/0.1 dl mixed with distilled water respectively. The various ratios of glucose (dextrose) concentration are (0, 15, 25, 50, 75, 100, 200, 300, 400, 500, 600, 700, 800, 900, 1000, 1100, 1200, 1300, 1400 and 1500 mg/dl). The next step is to position the each prepared samples (poured 3 ml volume) inside the sample holder of our prototype unit for their individual glucose concentration estimation. Eventually, the yield signals are stored for signal processing. The main task is to observe the variations of the peak amplitude values (mV) in the FFT domain corresponding to alteration in glucose concentration solutions.

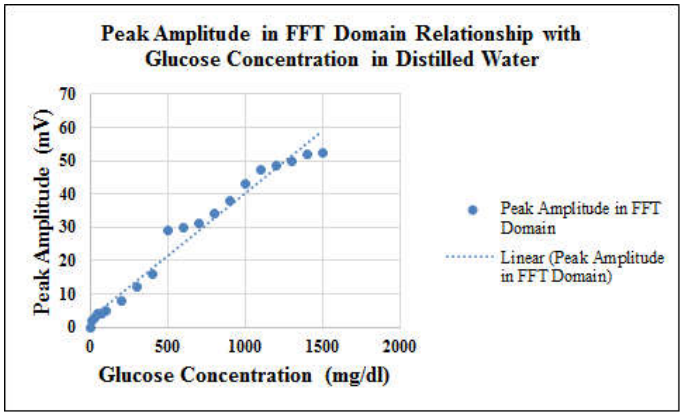

Figure 3.16: Peak-to-peak amplitude spectrum (in FFT domain) examined at 940 nm with different glucose concentration solutions.

3.3.1.1 Result analysis:

The figure 3.16 represents that peak-to-peak amplitude in FFT domain increases with respective increase in glucose concentrations, from 0 mg/dl to 1500 mg/dl res ectively.

3.3.2 *In-vitro* experiment using glucose in Intralipid™ phantom:

Our second step is to investigate the functioning of our modulated ultrasound and infrared light-based technique for glucose solution with Intralipid™ phantom based *in-vitro* studies. The different concentration of glucose like 0 mg/dl to 1500 mg/dl is mixed with Intralipid™ phantom for monitoring working of our technique. The stock solution of different ratio of dextrose anhydrous, purified powder from (Merck specialties private limited) 0 to 1500 mg/0.1 dl is mixed with distilled water. The prepared various concentration of glucose solution (0, 15, 25, 50, 75, 100, 200, 300, 400, 500, 600, 700, 800, 900, 1000, 1100, 1200, 1300, 1400 and 1500 mg/dl). Finally, the prepared 1 ml of glucose solution of different concentration mixed with 3 ml of Intralipid™ phantom sample was put inside the sample holder correspondingly.

Further, for investigation of the respective glucose concentration by our prototype unit, the output signals are stored for signal analysis. The main perception is to observe the variations of the peak amplitude values (mV) in the FFT domain regarding alteration in glucose concentration solutions mixed with Intralipid™ phantom.

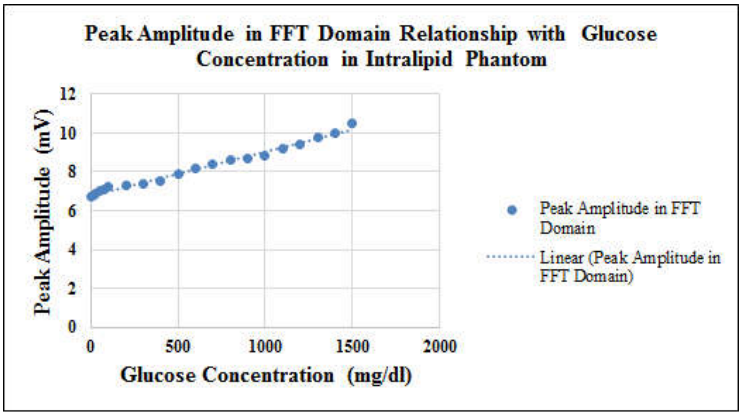

Figure 3.17: Peak-to-peak amplitude spectrum (in FFT domain) assessed at 940 nm from Intralipid™ phantom sample with different glucose concentrations.

3.3.2.1 Result analysis:

The figure 3.17 represents that peak-to-peak amplitude in FFT domain increases with respective increase in glucose concentrations mixed with Intralipid™ phantom sample, from 0 mg/dl to 1500 mg/dl respectively.

3.3.3 Our output signal of human blood plasma sample mixed with Intralipid™ phantom by modulated ultrasound and infrared (MUS-IR) unit:

In this present work, the *in-vitro* experiment performed on a human blood plasma samples mixed with Intralipid™ phantom medium for examining the output signal by our modulated ultrasound and infrared light based technique.

Table 3.9: The output signal parameters as acquired from the human blood plasma sample mixed with Intralipid™ phantom medium.

Characteristics of output wave signal	
CH1	50 mV
V_{pp}	132.0 mV
V_{rms}	74.0 mV
+Dut	53.00%
-Dut	47.00%
+wid	2.50 ms
-wid	2.22 ms

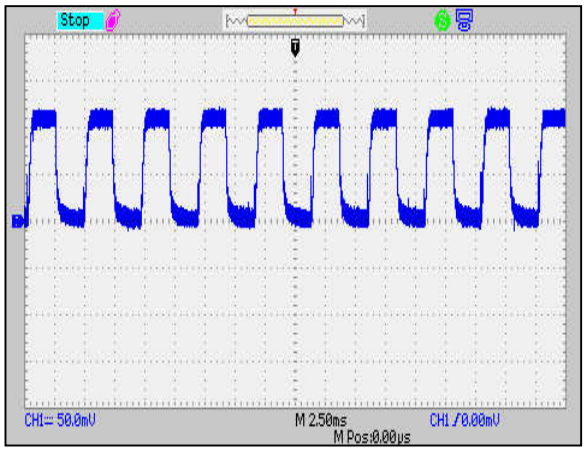

Figure 3.18: The output signal acquired from the human blood plasma sample mixed with Intralipid™ phantom medium.

The obtained signals are stored and examined for signal analysis. The figure 3.18 and Table 3.9 represents the DSO measured output signal, and its different parameters, as detected by the infrared photodiode of our prototype unit during the estimation of *in-vitro* samples with Intralipid™ phantom based study. The Table 3.9 represents in this present work, the CH1 (Channel 1 of DSO) has been chosen for this signal investigation. The V_{pp} and V_{rms} measured values are 132.0 mV and 74.0 mV respectively. Its +duty and -duty cycles has been 53.00% and 47.00% respectively. Further, its +width and -width has been 2.50 ms and 2.22 ms correspondingly.

3.3.4 *In-vitro* experiment using healthy and diabetic human blood samples mixed with Intralipid^{TM} phantom medium:

In this present work, our methodology includes preparing Intralipid^{TM} tissue phantom to mimic the finger absorption and scattering properties in the infrared spectral region. The healthy and diabetic human blood samples mixed with Intralipid^{TM} phantom medium used here to validate the functioning of our technique and for the calibration purpose. The different human blood samples are blood plasma, blood serum, whole blood sample respectively. The experiment was performed over three different volumes of Intralipid^{TM} phantom mediums such as 1 ml, 2 ml and 3 ml volumes. The investigation was performed at three different stages such as fasting, postprandial and random blood glucose analysis. The healthy and diabetic human blood plasma, blood serum and whole blood sample used here to investigate the blood glucose levels by our technique. Here *in-vitro* different human blood sample mixed with different ratio of Intralipid^{TM} phantom medium analysis performed, to explore the glucose sensitivity of our technique based prototype unit.

3.3.4.1 Study subjects:

Thirty adult subjects participated in this clinical examination. Fifteen subjects were healthy normal and fifteen subjects were diabetic with average age = 43±16 years, height = 168±4.0 cm, weight = 70±5.8 kg. Twenty-one subjects were male and nine subjects were female. The clinical studies reported here are as per the standard ethical methodology, performed with the informed consent of all the study subjects. The Ethical Committee of Institute of Medical Sciences-Banaras Hindu University, Varanasi permitted the clinical study.

3.3.4.2 Sample preparation:

The experiment was divided into three stages fasting, postprandial and random study on healthy normal and diabetic different human blood samples.

The sample preparation steps include:

Step 1. Preparation of human blood samples: The blood samples of 12 ml in quantity were collected at three times (overnight fasting stage, postprandial stage and random stage) from the veins of both right and left the arms of the subject for different types of blood sample preparations.

Step 2. Preparation of blood plasma sample: 05 ml of blood sample was collected in EDTA-treated vacuum-based blood collecting vials for preparation of

human blood plasma. The samples had undergone centrifugation procedure for 10 minutes. After centrifugation procedure, the supernatant fluid part of the sample had been collected as blood plasma. It had been stored for experimental purposes [Minh *et al.* (2011); Raghu (2003)].

Step 3. Preparation of blood serum sample: 05 ml of blood sample was collected in plain vial left in room temperature for 15-30 minutes for clotting process for preparation of human blood serum. The usually centrifugation techniques had been applied for clot breaking and serum collection. The Pasteur pipette had been used for serum fluid extraction from the vials and stored at 2°C to 8°C for investigational purposes [Raghu (2003)].

Step 4. Preparation of whole blood sample: 02 ml of blood was collected in vacutainer blood collecting vials containing anti-clotting agent like K_2 EDTA for preparation of whole blood sample. The phosphate buffer solution (PBS) had been used here for maintaining the pH level of the whole blood sample and stored for experimental purpose [Amir *et al.* (2007); Raghu (2003)].

Step 5. The three different (1 ml, 2 ml and 3 ml) volumes of Intralipid^{TM} phantom suspensions has been mixed with 1 ml of healthy normal and diabetic subjects blood plasma samples respectively.

Step 6: The three different (1 ml, 2 ml and 3 ml) volumes of Intralipid^{TM} phantom suspensions has been mixed with 1 ml of healthy normal and diabetic subjects blood serum samples respectively.

Step 7: The three different (1 ml, 2 ml and 3 ml) volumes of Intralipid^{TM} phantom suspensions has been mixed with 1 ml of healthy normal and diabetic subjects whole blood samples respectively.

Step 8. This step involves placing each prepared different *in-vitro* blood samples (blood plasma, blood serum, and whole blood) mixed Intralipid^{TM} phantom medium inside the sample holder of our prototype unit for its respective glucose concentration measurement.

In this present work, the various volumes (1 ml, 2 ml, and 3 ml) of the phantom medium have-been-used to investigate the calibration aspects, for measuring the glucose concentration in different prepared blood samples (blood plasma, blood serum, and whole blood) mixed Intralipid^{TM} phantom medium respectively. Based up on the experimental findings the Look-up Table has been prepared for correlating the

peak amplitude in FFT domain with the glucose concentration in the *in-vitro* samples (Provided in Appendix III to V).

3.3.4.3 Result analysis:

3.3.4.4 *In-vitro* analysis of the Intralipid^{TM} phantom mixed with blood plasma samples of the normal healthy subjects:

The figure 3.19 (a-c) depicts that the peak amplitude in FFT domain changes with respect to the change in the glucose concentration levels in the different volume based *in-vitro* samples. Three different volumes of *in-vitro* samples have been utilized here. Further, all the blood plasma samples belong to the fasting, postprandial and random stage based samples as obtained from the study subjects during clinical procedures respectively.

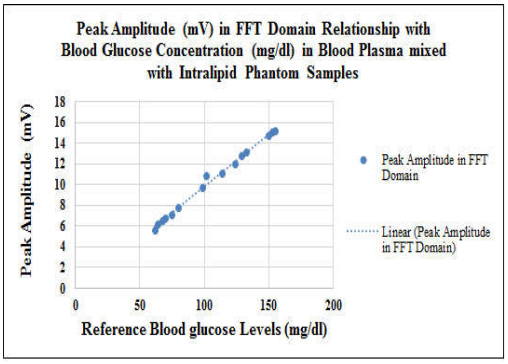

(a)

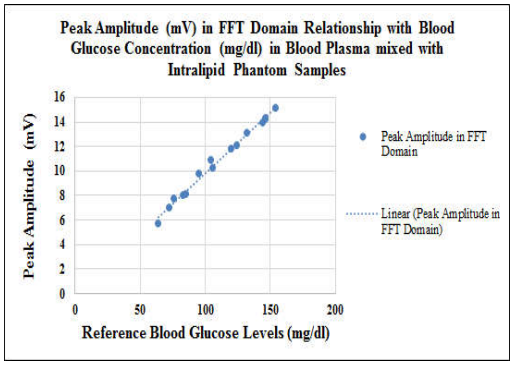

(b)

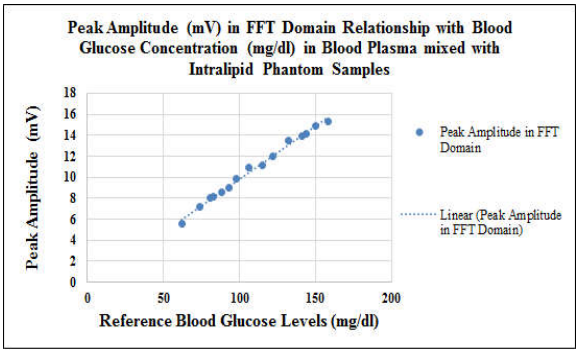

(c)

Figure 3.19 (a-c): The peak-to-peak amplitude in FFT domain relationship with the different glucose concentrations present in different volumes (1 ml, 2 ml, and 3 ml) of Intralipid^{TM} phantom samples mixed with healthy human blood plasma samples as obtained from the *in-vitro* samples of the study subjects during fasting, postprandial and random stages respectively.

The figure 3.19 (a) shows that the linear relationship exists between the peak amplitude in FFT domain with the glucose concentration present in 1 ml Intralipid^{TM} phantom suspension mixed with 1 ml of blood plasma samples. Similarly, the figure 3.19 (b) shows that the linear relationship exists between the peak amplitude in FFT domain with the glucose concentration present in 2 ml Intralipid^{TM} phantom suspension mixed with 1 ml of blood plasma samples. Likewise, the figure 3.19 (c) shows that linear relationship exists between the peak amplitude in FFT domain with the glucose concentration present in 3 ml Intralipid^{TM} Phantom suspension mixed with 1 ml of blood plasma samples.

Henceforth, in our proposed methods shows linear relationship with varying glucose concentration levels in different volumes of Intralipid^{TM} phantom suspension mixed blood plasma samples.

3.3.4.5 *In-vitro* analysis of the Intralipid^{TM} phantom mixed with blood plasma samples of the diabetic subjects:

The figure 3.20 (a-c) depicts that the peak amplitude in FFT domain changes with respect to the change in the glucose concentration levels in the different volume based *in-vitro* samples.

Three different volumes of *in-vitro* samples have been utilized here. Further, all the blood plasma samples as mentioned belong to the fasting, postprandial and random stage based samples obtained from the study subjects during clinical procedures respectively.

The figure 3.20 (a) shows that the linear relationship exists between the peak amplitude in FFT domain with the glucose concentration present in 1 ml Intralipid^{TM} phantom suspension mixed with 1 ml of blood plasma samples. Similarly, the figure 3.20 (b) shows the linear relationship between the peak amplitude in FFT domain with the glucose concentration present in 2 ml Intralipid^{TM} phantom suspension mixed with 1 ml of blood plasma samples. Likewise, the figure 3.20 (c) shows the linear relationship between the peak amplitude in FFT domain with the glucose concentration present in 3 ml Intralipid^{TM} phantom suspension mixed with 1 ml of blood plasma samples.

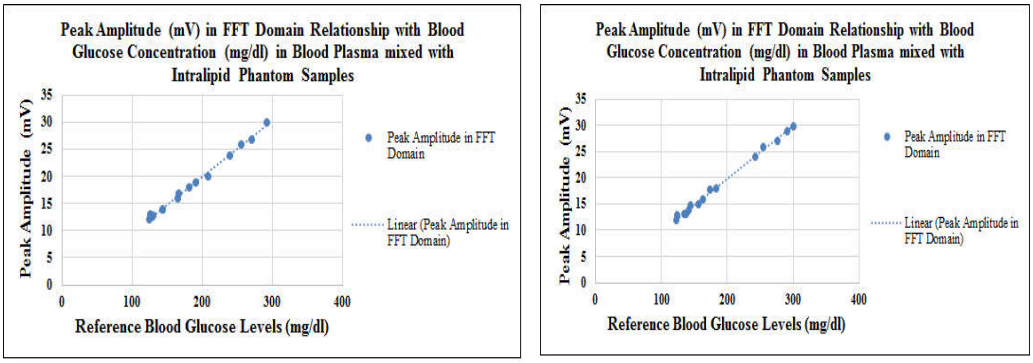

(a) **(b)**

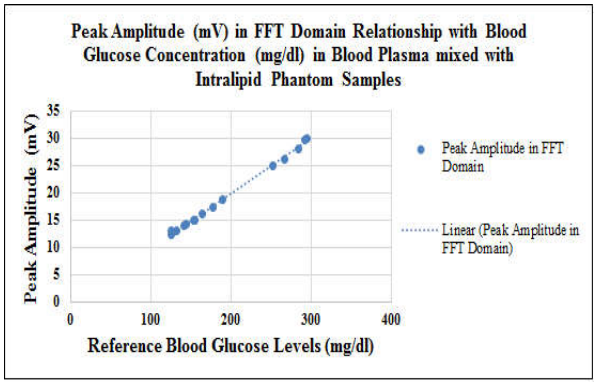

(c)

Figure 3.20 (a-c): The peak-to-peak amplitude in FFT domain relationship with the different glucose concentrations present in different volumes (1 ml, 2 ml, and 3 ml) of Intralipid^{TM} phantom samples mixed with diabetic human blood plasma samples as obtained from the *in-vitro* samples of the study subjects during fasting, postprandial and random stages respectively.

Henceforth, our proposed methods shows linear relationship with varying glucose concentration levels in different volumes of Intralipid^{TM} phantom suspension mixed blood plasma samples.

3.3.4.6 *In-vitro* analysis of the Intralipid^{TM} phantom mixed with blood serum samples of the normal healthy subjects:

The figure 3.21 (a-c) depicts that the peak amplitude in FFT domain changes with respect to the change in the glucose concentration levels in the different volume based *in-vitro* samples. Three different volumes of *in-vitro* samples have been utilized here. Further, all the blood serum samples as mentioned belong to the fasting, postprandial and random stage based samples obtained from the study subjects during

clinical procedures respectively. The figure 3.21 (a) shows the linear relationship between the peak amplitude in FFT domain with the glucose concentration present in 1 ml Intralipid^{TM} phantom suspension mixed with 1 ml of blood serum samples. Similarly, the figure 3.21 (b) shows that the linear relationship exists between the peak amplitude in FFT domain with the glucose concentration present in 2 ml Intralipid^{TM} phantom suspension mixed with 1 ml of blood serum samples. Likewise, the figure 3.21 (c) shows the linear relationship exists between the peak amplitude in FFT domain with the glucose concentration present in 3 ml Intralipid^{TM} phantom suspension mixed with 1 ml of blood serum samples.

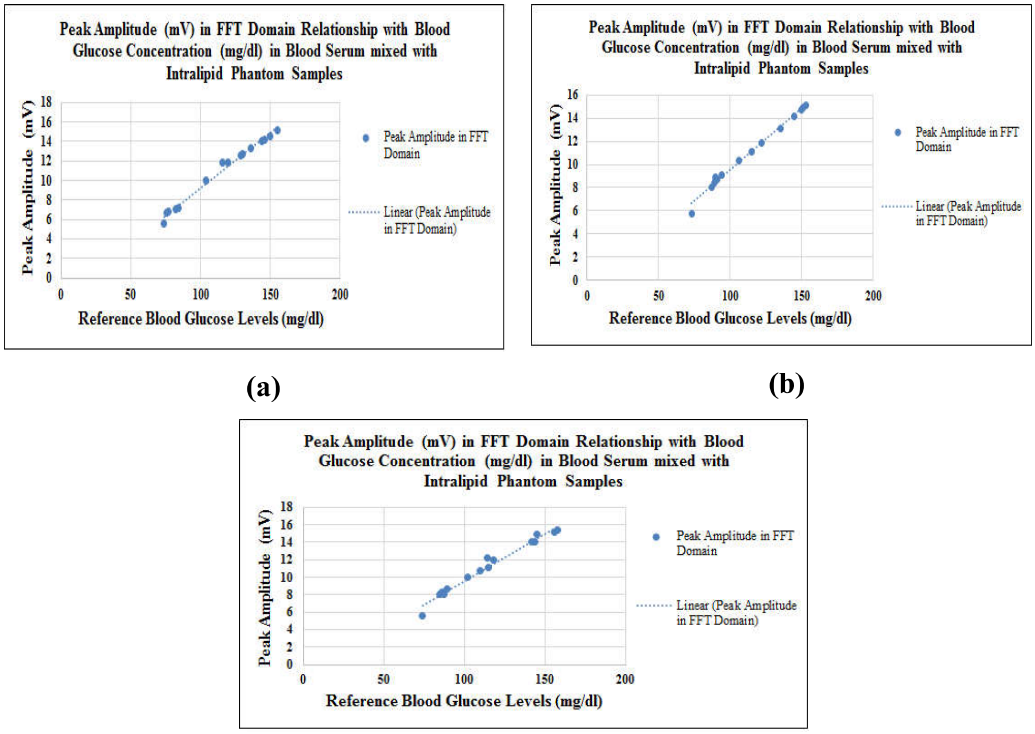

Figure 3.21 (a-c): The peak-to-peak amplitude in FFT domain relationship with the different glucose concentrations present in different volumes (1 ml, 2 ml, and 3 ml) of Intralipid^{TM} phantom samples mixed with healthy human blood serum samples as obtained from the *in-vitro* samples of the study subjects during fasting, postprandial and random stages respectively.

Henceforth, in our proposed methods shows linear relationship with varying glucose concentration levels in different volumes of Intralipid^{TM} phantom suspension mixed blood serum samples.

3.3.4.7 *In-vitro* analysis of the Intralipid^{TM} phantom mixed with blood serum samples of the diabetic subjects:

The figure 3.22 (a-c) depicts that the peak amplitude in FFT domain changes with respect to the change in the glucose concentration levels in the different volume based *in-vitro* samples. Three different volumes of *in-vitro* samples have been utilized here. Further, all the blood serum samples as mentioned belong to the fasting, postprandial and random stage based samples obtained from the study subjects during clinical procedures respectively.

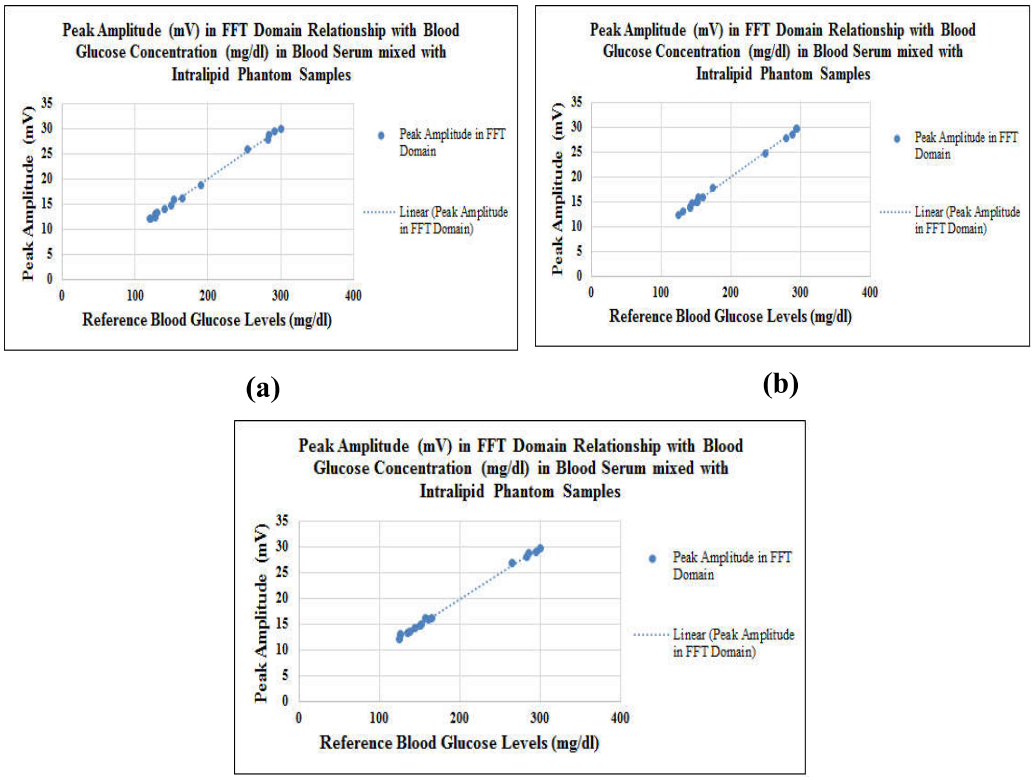

Figure 3.22 (a-c): The peak-to-peak amplitude in FFT domain relationship with the different glucose concentrations present in different volumes (1 ml, 2 ml, and 3 ml) of Intralipid^{TM} phantom samples mixed with diabetic human blood serum samples as obtained from the *in-vitro* samples of the study subjects during fasting, postprandial and random stages respectively.

The figure 3.22 (a) shows that the linear relationship exists between the peak amplitude in FFT domain with the glucose concentration present in 1 ml Intralipid^{TM} phantom suspension mixed with 1 ml of blood serum samples. Similarly, the figure 3.22 (b) shows the linear relationship between the peak amplitude in FFT domain with the glucose concentration present in 2 ml Intralipid^{TM} phantom suspension mixed with 1 ml of blood serum samples.

Likewise, the figure 3.22 (c) shows the linear relationship exists between the peak amplitude in FFT domain with the glucose concentration present in 3 ml Intralipid^{TM} phantom suspension mixed with 1 ml of blood serum samples. Henceforth, in our proposed methods shows linear relationship with varying glucose concentration levels in different volumes of Intralipid^{TM} phantom suspension mixed blood serum samples.

3.3.4.8 *In-vitro* analysis of the Intralipid^{TM} phantom mixed with whole blood samples of the normal healthy subjects:

The figure 3.23 (a-c) depicts that the peak amplitude in FFT domain changes with respect to the change in the glucose concentration levels in the different volume based *in-vitro* samples.

Three different volumes of *in-vitro* samples have been utilized here. Further, all the whole blood samples as mentioned belong to the fasting, postprandial and random stage based samples obtained from the study subjects during clinical procedures respectively.

The figure 3.23 (a) shows that the linear relationship exists between the peak amplitude in FFT domain with the glucose concentration present in 1 ml Intralipid^{TM} phantom suspension mixed with 1 ml of whole blood samples.

Similarly, the figure 3.23 (b) shows that the linear relationship exists between the peak amplitude in FFT domain with the glucose concentration present in 2 ml Intralipid^{TM} phantom suspension mixed with 1 ml of whole blood samples.

Likewise, the figure 3.23 (c) shows the linear relationship between the peak amplitude in FFT domain with the glucose concentration present in 3 ml Intralipid^{TM} phantom suspension mixed with 1 ml of whole blood samples.

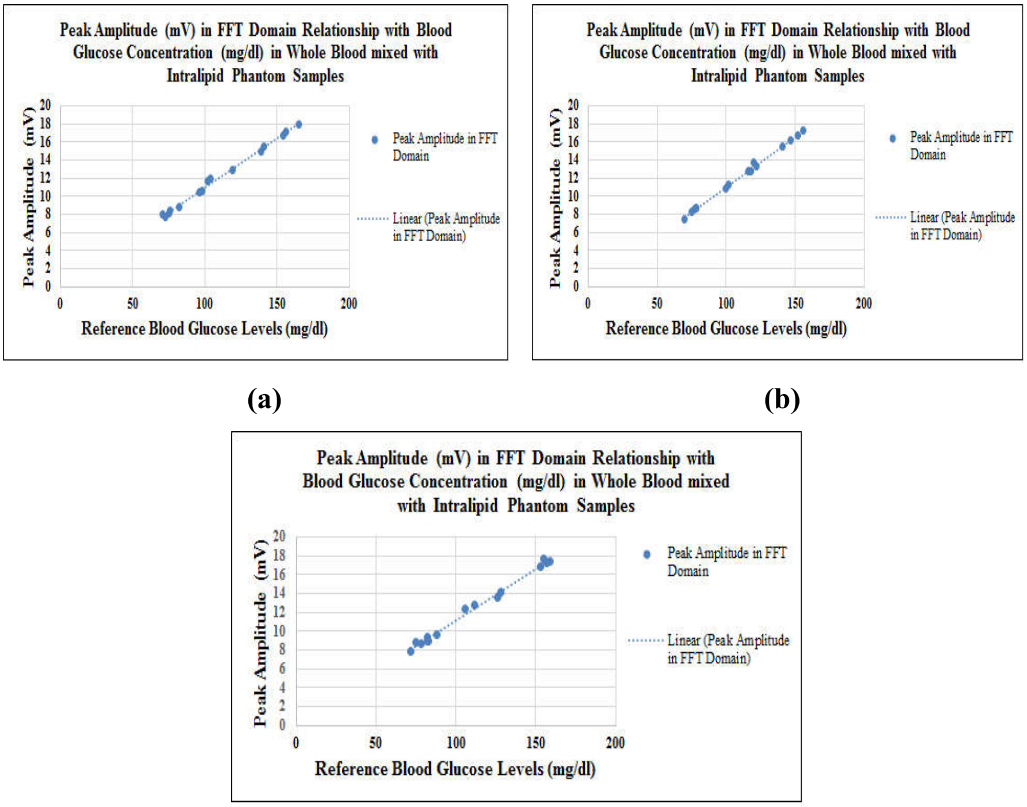

Figure 3.23 (a-c): The peak-to-peak amplitude in FFT domain relationship with the different glucose concentrations present in different volumes (1 ml, 2 ml, and 3 ml) of Intralipid^{TM} phantom samples mixed with healthy human whole blood samples as obtained from the *in-vitro* samples of the study subjects during fasting, postprandial and random stages respectively.

Henceforth, in our proposed methods shows linear relationship with varying glucose concentration levels in different volumes of Intralipid^{TM} phantom suspension mixed whole blood samples.

3.3.4.9 *In-vitro* analysis of the Intralipid^{TM} phantom mixed with whole blood samples of the diabetic subjects:

The figure 3.24 (a-c) depicts that the peak amplitude in FFT domain changes with respect to the change in the glucose concentration levels in the different volume based *in-vitro* samples.

Three different volumes of *in-vitro* samples have been utilized here. Further, all the whole blood samples as mentioned belong to the fasting, postprandial and

random stage based samples obtained from the study subjects during clinical procedures respectively. The figure 3.24 (a) shows that the linear relationship exists between the peak amplitude in FFT domain with the glucose concentration present in 1 ml Intralipid^{TM} phantom suspension mixed with 1 ml of whole blood samples. Similarly, the figure 3.24 (b) shows that the linear relationship exists between the peak amplitude in FFT domain with the glucose concentration present in 2 ml Intralipid^{TM} phantom suspension mixed with 1 ml of whole blood samples. Likewise, the figure 3.24 (c) shows the linear relationship exists between the peak amplitude in FFT domain with the glucose concentration present in 3 ml Intralipid^{TM} phantom suspension mixed with 1 ml of whole blood samples.

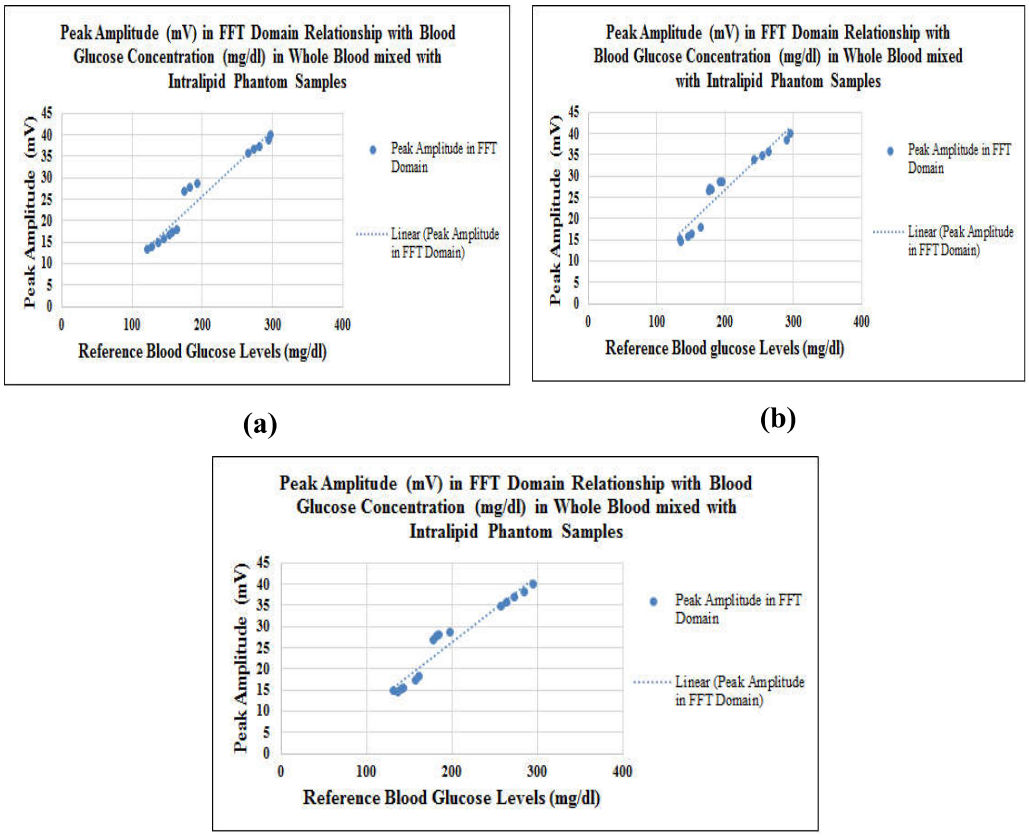

Figure 3.24 (a-c): The peak-to-peak amplitude in FFT domain relationship with the different glucose concentrations present in different volumes (1 ml, 2 ml, and 3 ml) of Intralipid^{TM} phantom samples mixed with diabetic human whole blood samples as obtained from the *in-vitro* samples of the study subjects during fasting, postprandial and random stages respectively.

Henceforth, in our proposed methods shows linear relationship with varying glucose concentration levels in different volumes of Intralipid^{TM} phantom suspension mixed whole blood samples.

These correlated variations specify the direction of the sensitivity (at 940 nm wavelength) of our prototype unit in sensing glucose concentration variation in respective different human blood samples mixed with different ratio of Intralipid^{TM} phantom medium. The experimental detailed illustration of this phenomenon has-been- in chapter 5, of this present thesis works.

The peak amplitude increases with increase in blood glucose levels, this phenomenon depicts the glucose concentration induced light clearing effects. The experimental illustration of this phenomenon has-been-described in chapter 4 of this present thesis work. The *in-vitro* examination represents strong correlation between examined glucose levels and the real concentration. Henceforth this phenomenon forms the benchmark and base for performing the *in-vitro* examinations to develop the performance and efficiency of our technique for glucose estimation.

3.4 Extended *in-vitro* clinical examination:

This present work represents the effect of absence and presence of amplitude modulated ultrasonic waves. The effect of ultrasound examined by performing the different human blood samples mixed with Intralipid^{TM} based tissue phantom. The specific effect of ultrasound is observed by using infrared LED of 940 nm. The experimental design and resultant output in Fast Fourier Transform Domain for glucose prediction in different human blood samples mixed with Intralipid^{TM} based tissue phantom had been described in this present work. This technique will assist in performing calibration aspects for our technique based *in-vitro* blood glucose estimations.

3.4.1 Study subject:

The male subject age is around 26 years, height of 158 cm and weight of 72 kg. The experimental protocols were described to the subject. He understood the process and gave the consent. The local ethical committee had approved the study. The blood sample for blood plasma, blood serum and whole blood preparation had been collected from a normal male subject for experimental purposes.

3.4.2 Preparation of human blood samples:

The blood samples of 10 ml in quantity were drawn for two times (overnight fasting and postprandial stage) from the veins of right arm of the subject for various types of blood sample preparations.

3.4.3 Blood plasma sample preparation:

For human blood plasma preparation, 4 ml of blood sample had been collected in EDTA-treated vacuum-based blood collecting vials. The samples had been applied to standard centrifugation process for 10 minutes. After centrifugation process, the supernatant fluid part of the sample had been collected as blood plasma. It had been stored for experimental purposes [Minh *et al.* (2011); Raghu (2003)].

3.4.4 Blood serum sample preparation:

For human blood serum preparation, the 4 ml of blood sample had been stored room temperature for 15-30 minutes for clotting process. Usually centrifugation methods had been applied for clot breaking and serum collection. The pasture pipette had been used for serum fluid extraction from the vials and stored at 2°C to 8°C for experimental purposes [Raghu (2003)].

3.4.5 Whole blood sample preparation:

For whole blood sample preparation, the 2 ml of blood had been collected in vacutainer blood collecting vials containing anti-clotting agent like K_2 Ethylene Di-amine Tetra-acetic Acid (EDTA). Phosphate buffer solution (PBS) had been utilized here for maintaining the pH level of the whole blood sample [Amir *et al.* (2007); Raghu (2003)]. After that, it was stored for experimental works.

3.4.6 Result analysis:

The experiments were performed in four stages and results including figure 3.25 to 3.32 are described in this present work.

3.4.6.1 Stage I:

In this part, the 2 ml of Intralipid^{TM} sample had been taken in sample test tube from the Intralipid^{TM} stock suspension using micropipette. The Intralipid^{TM} sample filled test tubes had been inserted in the sample holder of the modulated ultrasound with infrared (MUS-IR) unit. Both measurement in absence and presence of ultrasound had been conducted. Intralipid^{TM} (tissue phantom) had been used here as a blank and for calibration purposes. The observed signal and its Fast Fourier Transform (FFT) were performed and stored electronically for analytical purposes.

The figure 3.25 (a), 3.26 (a) and figure 3.25 (b), 3.26 (b) shows both the observed signals, FFT domain peak amplitude spectrum in absence and presence of ultrasound in MUS-IR unit respectively. The comparison of figure 3.25 (a) and figure 3.26 (a) of the observed signal reveals that the wave pattern characteristics changes when ultrasonic mode had been applied in MUS-IR unit.

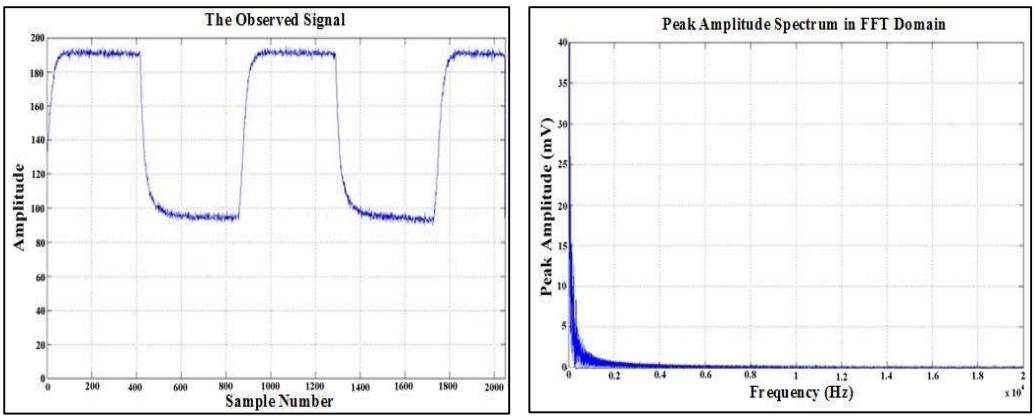

(a) **(b)**

Figure 3.25 (a): Shows the observed signal **(b)** its corresponding peak amplitude in FFT domain of the Intralipid^{TM} sample as a blank in absence of ultrasound in MUS-IR unit.

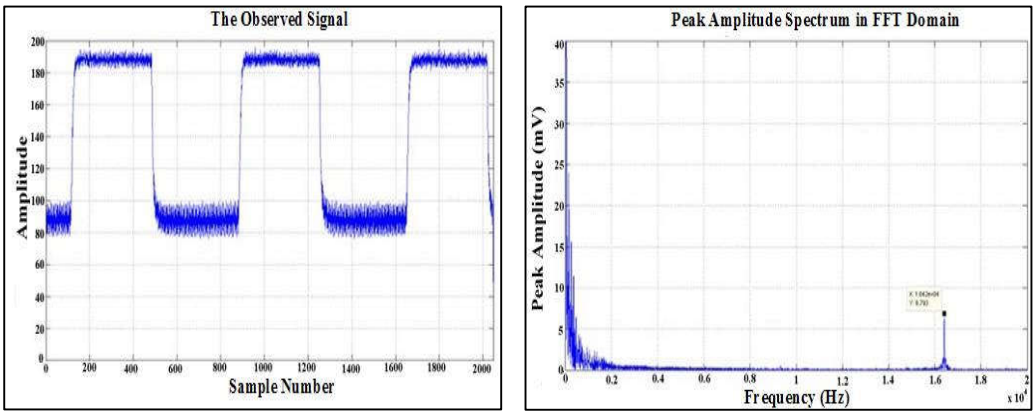

(a) **(b)**

Figure 3.26 (a): Shows the observed signal **(b)** its corresponding peak amplitude spectrum in FFT domain of Intralipid^{TM} sample as a blank in presence of ultrasound in MUS-IR unit.

Figure 3.25 (b) in Fast Fourier Transform (FFT) domain the peak amplitude was not seen in absence of ultrasound. On the contrary, figure 3.26 (b) reveal that the peak amplitude spectrum of blank Intralipid^{TM} had been observed in FFT domain when ultrasound is present in MUS-IR unit and the peak amplitude value is 6.7 mV. This indicates the significant working of ultrasound in MUS-IR unit.

3.4.6.2 Stage II:

During this part, 1 ml of human blood fasting plasma sample as prepared had been added to 1 ml of Intralipid^{TM} suspension. Similarly, 1 ml of human blood postprandial plasma sample is added to another 1 ml of Intralipid^{TM} suspension. Both the fasting and postprandial samples were examined respectively in presence of ultrasound through modulated ultrasound with infrared (MUS-IR) unit. The results of the observed signal and peak amplitude spectrum in FFT domain in presence of ultrasound were captured and stored. The figure 3.27 (a), 3.28 (a) and figure 3.27 (b), 3.28 (b) shows both the fasting and postprandial blood plasma in Intralipid^{TM} suspension samples of the observed signals, FFT domain peak amplitude spectrum in presence of ultrasound in MUS-IR unit respectively. The wave pattern changes were revealed when figure 3.27 (a) and 3.28 (a) were observed. Similarly, from figure 3.27 (b) the peak amplitude value is 7.5 mV and figure 3.28 (b) the peak amplitude value is 10.3 mV of fasting and postprandial blood plasma samples respectively.

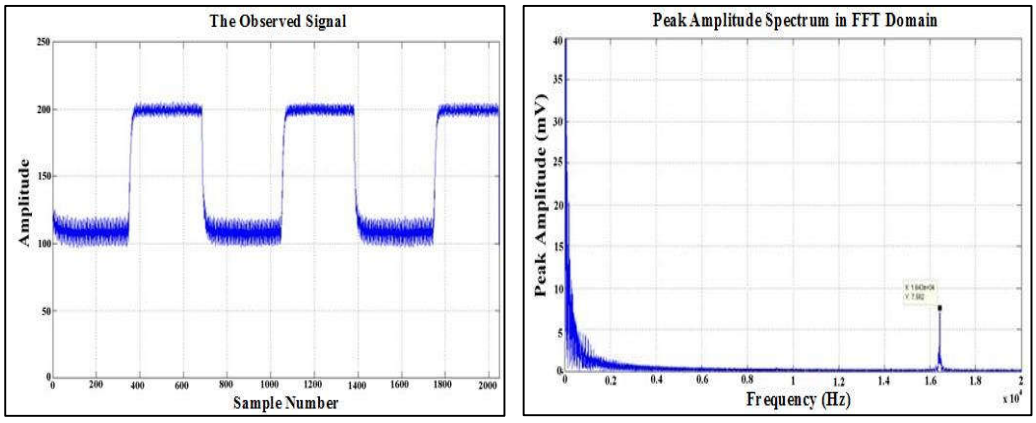

(a) **(b)**

Figure 3.27 (a): Shows the observed signal **(b)** its corresponding peak amplitude spectrum in FFT domain of fasting plasma mixed Intralipid^{TM} sample in presence of ultrasound in MUS-IR unit.

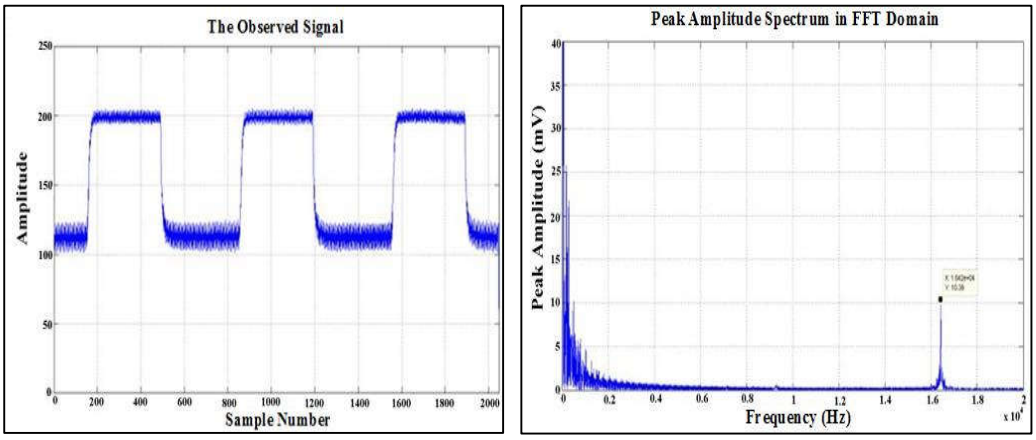

(a) **(b)**

Figure 3.28 (a): Shows the observed signal **(b)** its corresponding peak amplitude spectrum in FFT domain of postprandial plasma mixed Intralipid^{TM} sample in presence of ultrasound in MUS-IR unit.

The peak amplitude value varies with change in blood glucose concentrations. The postprandial blood plasma sample peak amplitude in FFT domain were on higher side as compared to the fasting blood plasma mixed Intralipid^{TM} sample respectively.

3.4.6.3 Stage III:

This part belongs to the modulated ultrasound with infrared (MUS-IR) unit based experimentation including 1 ml of fasting blood serum with 1 ml Intralipid^{TM} suspension and 1 ml of postprandial human blood serum sample mixed with 1ml Intralipid^{TM} suspension respectively. Outputs of the experimentation were recorded for analysis. The figure 3.29 (a), 3.30 (a) and figure 3.29 (b), 3.30 (b) shows both the fasting and postprandial blood serum in Intralipid^{TM} suspension samples of the observed signals, FFT domain peak amplitude spectrum in presence of ultrasound in MUS-IR unit respectively. The figure 3.29 (a) and 3.30 (a) shows that they vary in their wave pattern characteristics when compared.

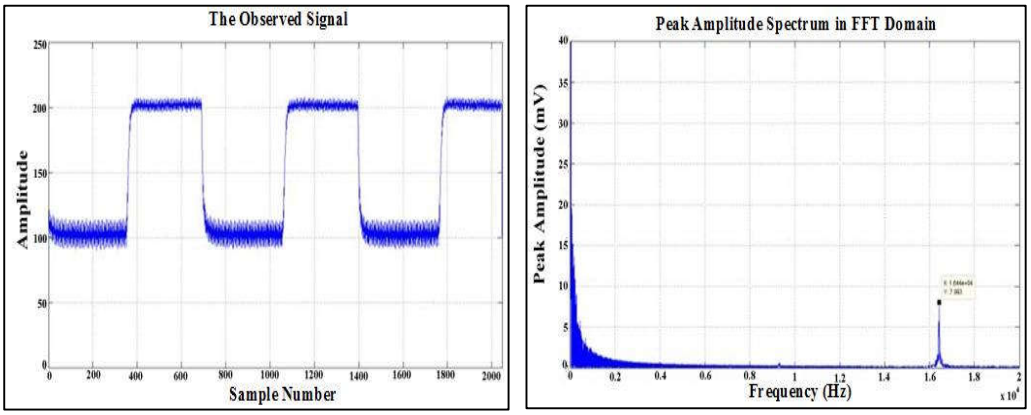

(a) **(b)**

Figure 3.29 (a): Shows the observed signal **(b)** its corresponding peak amplitude spectrum in FFT domain of fasting serum mixed Intralipid^{TM} sample in presence of ultrasound in MUS-IR unit.

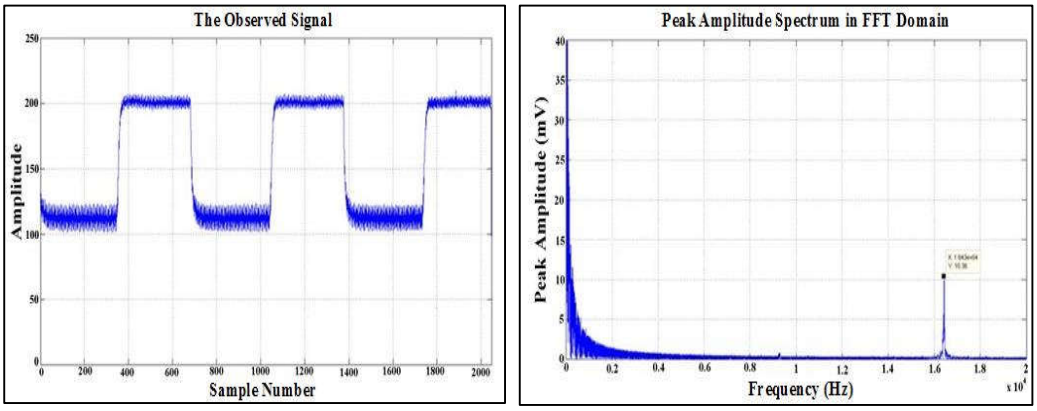

(a) **(b)**

Figure 3.30 (a): Shows the observed signal **(b)** its corresponding peak amplitude spectrum in FFT domain of postprandial serum mixed Intralipid^{TM} sample in presence of ultrasound in MUS-IR unit.

Similarly, from figure 3.29 (b) the peak amplitude value is 7.9 mV and figure 3.30 (b) the peak amplitude value is 10.3 mV of fasting and postprandial blood serum samples respectively. The peak values were in increasing mode in postprandial serum sample as compared to the fasting serum sample mixed Intralipid^{TM} suspension respectively.

3.4.6.4 Stage IV:

In this portion the modulated ultrasound with infrared (MUS-IR) unit based experimentation were conducted utilizing 1 ml of fasting whole blood sample with 1 ml of Intralipid^{TM} suspension and 1 ml of postprandial human blood whole blood sample mixed with 1 ml Intralipid^{TM} suspension respectively. The resultants of observed signals were stored for analytical purposes.

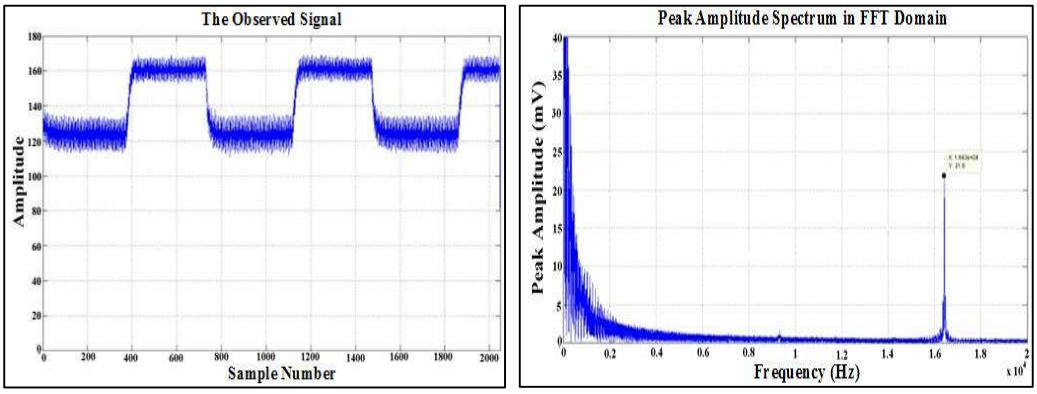

(a) **(b)**

Figure 3.31 (a): Shows the observed signal **(b)** its corresponding peak amplitude spectrum in FFT domain of fasting whole blood mixed Intralipid^{TM} sample in presence of ultrasound in MUS-IR unit.

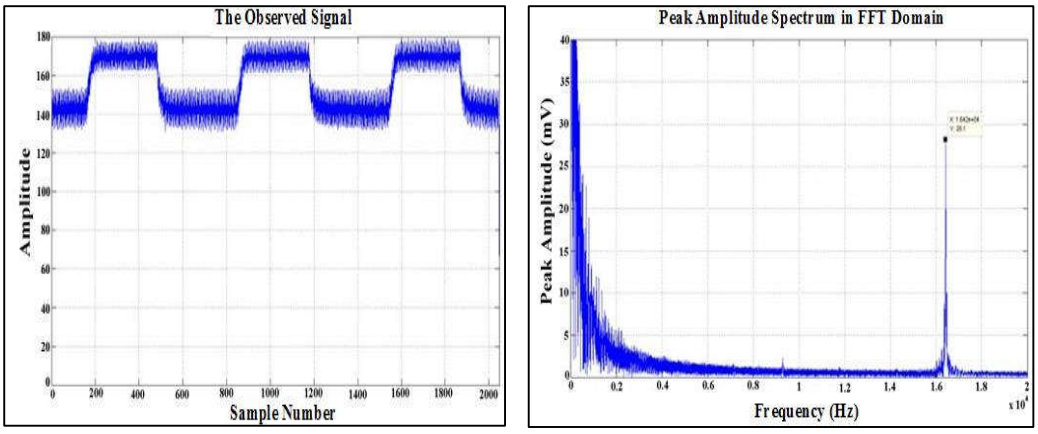

(a) **(b)**

Figure 3.32 (a): Shows the observed signal **(b)** its corresponding peak amplitude spectrum in FFT domain of postprandial whole blood mixed Intralipid^{TM} sample in presence of ultrasound in MUS-IR unit.

The figure 3.31 (a), 3.32 (a) and figure 3.31 (b), 3.32 (b) shows both the fasting and postprandial whole blood sample in Intralipid™ suspension samples observed signals, FFT domain peak amplitude spectrum in presence of ultrasound in MUS-IR unit respectively. The wave shape characteristics vary in figure 3.31 (a) and 3.32 (a) when evaluated. The phenomenon of glucose concentration variation causes changes in the peak amplitude in FFT domain as seen in figure 3.31 (b) the peak amplitude value is 21.8 mV and figure 3.32 (b) the peak amplitude value is 28.1 mV respectively. The postprandial whole blood mixed Intralipid™ sample occupies higher peak values than the fasting results respectively.

3.4.7 Conclusion:

The MUS-IR unit had been utilized here for glucose concentration determinations in various human blood samples like blood plasma, blood serum, whole blood mixed with Intralipid™ tissue phantom. The results indicate that ultrasound performs a key role in determining glucose concentrations in fasting and postprandial samples. This principle would be useful for calibration purpose and significant direction of blood glucose estimation.

3.5 Calibration:

The peak amplitude in the FFT domain corresponds to the blood glucose concentration in different human blood mixed Intralipid™ phantom samples. The product of Calibration Factor (CF) and peak amplitude (mV) in the FFT domain predicts blood glucose concentration in mg/dl and is scientifically expressed here as:

$$V_{peak} \times CF = PBGL \qquad \text{Equation (3.4)}$$

Where, V_{peak} stands for peak voltage amplitude (mV) in FFT domain, CF stands for Calibration Factor, and PBGL refers to Predicted Blood Glucose Level in mg/dl.

3.6 Inference:

Henceforth, this part reports the glucose concentration associated sensitivity of our *in-vitro* approach. The efficient correlation between the patterns of peak amplitude (mV) in FFT domain spectrum with varying blood glucose levels verifies the feasibility of this new approach. By implementing such phenomenon, we performed different *in-vitro* blood glucose estimation based clinical examination in

human blood samples and this technique has been described in the chapter 5 of this present thesis.

3.7 Tests methodology:

For developing the clinical accuracy and establishing capability of our MUS-IR technique is a complex job. To verify our technique, we have conducted a clinical examination that contains OGTT (Oral Glucose Tolerance Tests), Fasting blood glucose analysis, Postprandial blood glucose analysis and Random blood glucose analysis on normal and diabetic study subjects by using the principle of GOD/POD method and invasive glucometer.

3.7.1 Principle of GOD/POD method:

The experimental reference value Blood Glucose Level (BGL) obtained by GOD/POD method during the *in-vitro* examination of human blood samples. Glucose is oxidized by the glucose oxidase (GOD) to produce gluconate and hydrogen peroxide. The hydrogen peroxide is then oxidatively combined with 4 amino-antipyrene (4-AAP) and phenol in the presence of peroxidase (POD) to produce a red quinoeimine color that is assessed at 505 nm wavelength. The absorbance at 505 nm is corresponding to the concentration of glucose present in the sample [Kirschner *et al.* (2001); McMurry *et al.* (1998); Trinder (1969)].

$$\text{Glucose} + 2H_2O + O_2 \xrightarrow{\text{GOD}} \text{Gluconate} + H_2O_2$$

$$2H_2O_2 + \text{4-AAP} + \text{Phenol} \xrightarrow{\text{POD}} \text{Quinoeimine Dye}$$

Absorbance of the colored solution is directly proportional to the glucose concentration, when measure at the wavelength of 505 nm.

3.7.1.1 Procedure:

The Table 3.10 illustrated the utilization of Reagent 1 as blank and Reagent 2 as standard are sufficient for each assay series.

Table 3.10: Showing the volume of reagent and sample into test tubes.

Particulars	Blank	Standard	Sample
Reagent 1	1000 µl	1000 µl	1000 µl
Distill Water	10 µl	-	-
Reagent 2	-	10 µl	-
Sample	-	-	10 µl

Properly mix the sample and incubate for 15 minutes at room temperature or 7 minutes at 37°C. Measure the absorbance of standard (A std) and sample (A sample) against reagent blank at 505 nm wavelength. All the measurement are performed on Digital spectrophotometer.

3.7.1.2 Calculation:

Glucose concentration in the sample can be calculated by using this following formula:

$$\text{Glucose (mg/dl)} = \frac{\text{Absorbance of Sample}}{\text{Absorbance of Standard}} \text{ X } \frac{\text{Concentration of}}{\text{Standard (mg/dl)}}$$

3.7.2 Invasive glucometer:

The Accu-Check Active Invasive Glucometer of Roche Diagnostics GmbH, Manheim, Germany used in some experimental process for cross check purpose. The Roche Diagnostics, GmbH, Manheim, Germany estimating the accuracy of the Accu-Chek Active system according to the ISO (International Organization for Standardization) 15197, and the Accu-Chek Active system meets the exactness necessity for the ISO 15197 standard [ISO_Active_EN, (2006); Lam (2008)].

3.7.3 Our prototype unit:

The figure 3.33 represents complete system of our prototype unit for *in-vitro* blood glucose estimation. Similarly, the figure 3.34 represents *in-vitro* sample measurements processes.

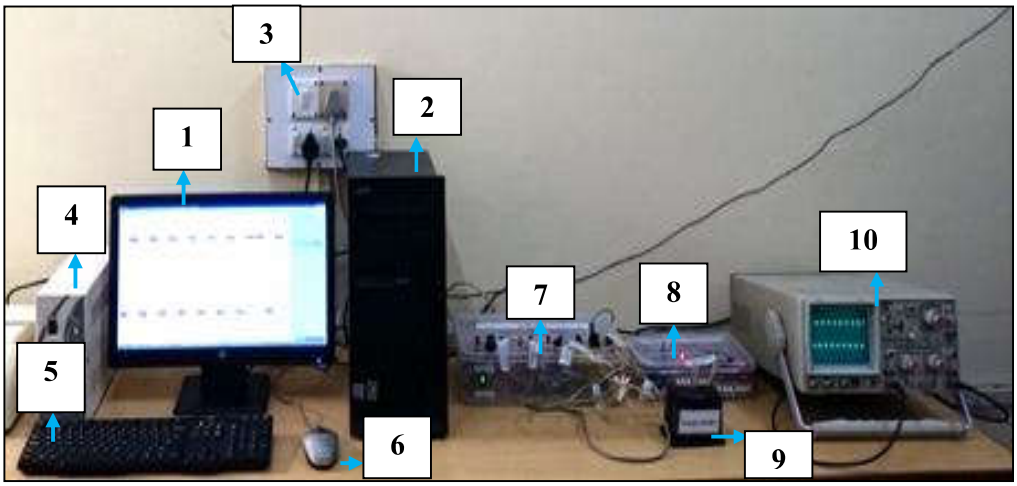

Figure 3.33: Our *In-vitro* technique based prototype (MUS-IR) unit;
1. Computer display, 2. Central Processing Unit, 3. Main Power Supply, 4. UPS, 5. Keyboard, 6. Mouse, 7. Modulating wave supply unit and MUS-IR unit, 8. Carrier wave supply unit, 9. Sample holder, 10. Oscilloscope.

In this present work, for *in-vitro* Blood Glucose Level estimation (referred here as the Predicted Blood Glucose Level) in study subjects the aforementioned *in-vitro* technique based prototype unit is used.

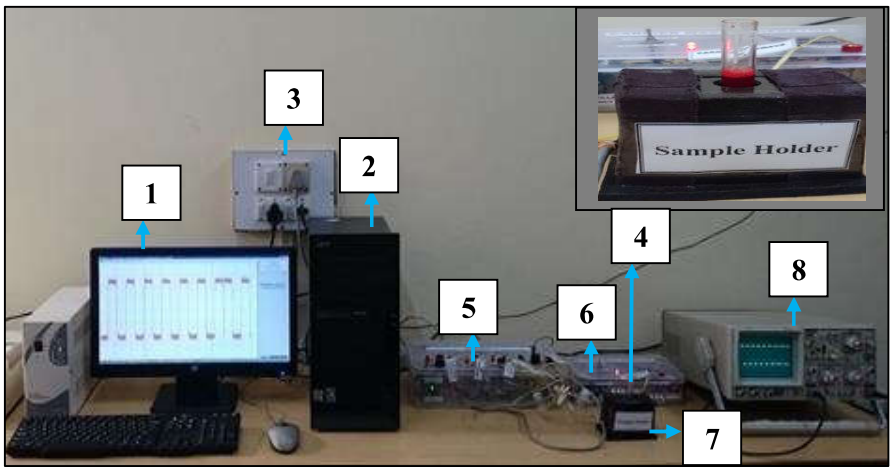

Figure 3.34: Our *in-vitro* technique based prototype unit for Predicted Blood Glucose Level measurement in human blood samples.

1. Spectral reading program with computer, 2. Central Processing Unit, 3. Main Power Supply, 4. Examine blood sample, 5. Modulating wave supply unit and MUS-IR unit, 6. Carrier wave supply unit, 7. Sample holder, 8. Signal acquisition by an oscilloscope and transferring it to the computer for Predicted (*In-vitro*) Blood Glucose Level measurement.

The Ethical Committee of Institute of Medical Sciences, Banaras Hindu University, Varanasi, ethically endorsed all the *in-vitro* human blood samples studied in this present work.

3.8 Performance assessment technique:

For the validation and analysis of our present work, we have adopted following methods of analysis in our thesis work:

(i) Clarke Error Grid analysis

(ii) Parkes Error Grid analysis

(iii) Statistical analysis

3.8.1 Clarke Error Grid analysis:

The Clarke Error Grid investigation is the general method for assessing medical importance of the developing glucose sensor based procedures for blood

glucose estimation. In this present work, the Clarke Error Grid analysis significantly assesses the medically significance of the variations between our *in-vitro* (as predicted by our prototype unit) system based blood glucose levels as the predicted technique under examination and established GOD/POD method based blood glucose level estimation as the reference method. Clarke *et al.* (1987) introduced this approach utilizing the Cartesian diagram to compute the predicted blood glucose values against the established invasive technique (real) blood glucose values. For example, when the predicted blood glucose value is 126 mg/dl and the reference blood glucose value acquired is 91 mg/dl, the Cartesian XY coordinates represents it as (91,126) respectively. In this form, the diagonal line where X=Y, expresses the ideal estimations. The data points under and over the diagonal line presents to the overestimation and underestimation of the real blood glucose values respectively. Additionally, when any data pair fall on the borderline of any zones, the nearness of its (X, Y) coordinate towards either zone decides its zone of its occupancy [Hidalgo *et al.* (2014); Clarke *et al.* (1987)].

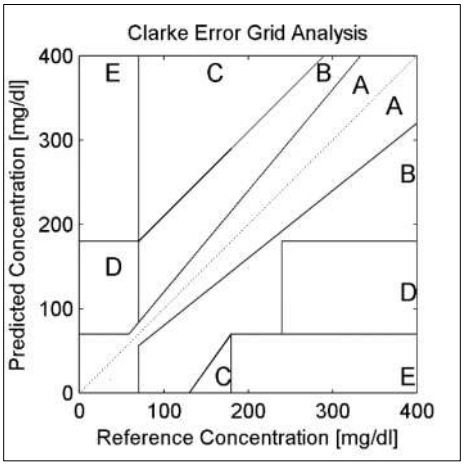

Figure 3.35: Clarke Error Grid plot [Clarke *et al.* (1987)].

Further, on the basis of the degree of miss calculation, the XY-Cartesian graph includes different grid zones. As represent in figure 3.35, the Clarke Error Grid include of five different zones in the XY-Cartesian graph with the following elucidations [Hidalgo *et al.* (2014); Clarke *et al.* (1987)].

Zone A [Medically accurate]: Distinguishes the blood glucose values that deviate away from the real reference values by means of 20% or less. This zone also

contains hypoglycemic blood glucose values (below the 70 mg/dl). The yield values in this zones are medically accurate and medical attention will be appropriate [Hidalgo *et al.* (2014); Clarke *et al.* (1987)].

Zone B [Medically significant and acceptable]: Distinguishes the blood glucose values that deviate from the real reference values by means for more than 20%. This domain represents the beginning of errors but medical treatment includes a high probability of being accurate. The data points under the Zone B may also be medically significant and tolerable [Hidalgo *et al.* (2014); Clarke *et al.* (1987)].

Zone C-E [Medically insignificant and potentially dangerous]: The blood glucose values in these zones presents potentially dangerous and unsatisfactory estimations. While the predicted values are far from the reference values, the medical treatment predicated on these outcomes will be incorrect and includes high risk [Hidalgo *et al.* (2014); Clarke *et al.* (1987)].

3.8.2 Parkes Error Grid analysis:

Parkes *et al.* (2000) explored the idea of particular zones and composed a new arrangement of inventive errors grids (also called as Consensus Error Grid), in view of the ability of large group of medical specialists. These new Error Grids were composed distinguishing for Type I and Type II diabetic subjects. Parkes Error Grids had been divided into 05 sections, for example, Zone A to Zone E respectively [Hidalgo *et al.* (2014); Pfutzner *et al.* (2013)].

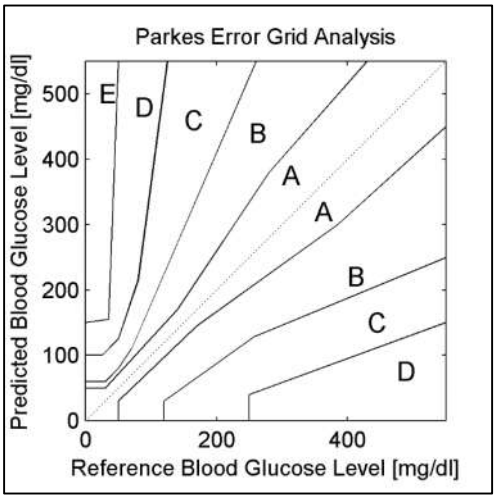

Figure 3.36: Parkes Error Grid plot [Parkes *et al.* (2000)].

The figure 3.36 represents the Parkes Error Grid include of five different zones in the XY-Cartesian graph with the following elucidations [Hidalgo *et al.* (2014); Pfutzner *et al.* (2013); Parkes *et al.* (2000)].

Zone A: implies medically accurate determinations, with no significance over medical supervision.

Zone B: implies changed medical action, little or no significance over medical treatment.

Zone C: implies changed medical action, likely to influence medical treatment.

Zone D: implies changed medical action, may contain imperative medical risk.

Zone E: implies changed medical action, may contain risky effects.

3.8.3 Statistical analysis:

In this present work, different statistical performance metrics based parameter performs accuracy assess examinations for correlating real invasive blood glucose levels with the evaluated blood glucose levels and the outputs provides promising results.

In this, different statistical performance evaluation parameters mostly contains (i) Pearson Correlation Coefficient (r value), (ii) SEP (Standard Error of Prediction), (iii) Mean Absolute Error (MAE), (iv) Median Absolute Error (MdAE),(v) Root Mean Squared Error (RMSE), (vi) Percentage of Mean Absolute Relative Error (%MARE), (vii) Percentage of Median Absolute Relative Error (%MdARE).

The Table 3.11 presents to the mathematical expressions of the accuracy evaluation parameters used in this experimental work for the total number of sample data pairs. Overall these accuracy measure assesses the accuracy of predicted blood glucose levels concerning the reference establish invasive blood glucose levels.

Further, to evaluate the statistical significance of our outcomes different statistical analysis techniques Deming Regression, CUSUM test for linearity, Paired sample t-tests, Mountain Plot, Bland Altman Plot, Rank Correlation, Pearson Correlation Coefficient (r-value), Clarke and Parkes Error Grids, Accuracy measure are used over our overall clinical examination based results.

Table 3.11: Performance evaluation parameters.

Accuracy Measure	Mathematical Expression	Symbol Notations	References
Pearson Correlation Coefficient (r-value)	The correlation (r) between $x$and y is: $r = \frac{1}{n-1}\sum_{i=1}^{n}\left(\frac{x_i-\bar{x}}{s_x}\right)\left(\frac{y_i-\bar{y}}{s_y}\right)$ $= \frac{\sum_{i=1}^{n}(x_i-\bar{x})\,(y_i-\bar{y})}{\sqrt{\sum_{1=1}^{n}(x_i-\bar{x})^2(y_i-\bar{y})^2}}$	Where x represents RBGL value, y represent PBGL value and, n represents the total number of sample pairs. The mean and standard deviations of the two variables are $\bar{x}$ and s_x for x values, and $\bar{y}$ and s_y for y values.	Sharma (2012)
SEP (Standard Error of Prediction)	The equation for the standard error of the predicted y is: $\sqrt{\frac{1}{(n-2)}\left[\sum(y-\hat{y})^2-\frac{[\sum(x-\hat{x})\,(y-\hat{y})]^2}{\sum(x-\hat{x})^2}\right]}$	Where x and y are the sample means AVERAGE (known_x's) and AVERAGE (known_y's), and n is the sample size.	Jelen (2013)
MAE (Mean Absolute Error)	$MAE = \frac{\sum_{i=1}^{N}\lvert y_i-\hat{y}_i\rvert}{N}$	Where y_i is the Reference Blood Glucose Level (RBGL) value, $\hat{y}_i$ is the Predicted Blood Glucose Level (PBGL) value, and N represents the total number of sample pairs.	Hariri *et al.* (2011); Shcherbakov *et al.* (2013); Guevara *et al.* (2010); Facchinetti *et al.* (2007).
MdAE (Median Absolute Error)	$MdAE = median\sum_{i=1}^{N}\lvert y_i-\hat{y}_i\rvert$		
RMSE (Root Mean Squared Error)	$RMSE = \sqrt{\frac{\sum_{i=1}^{N}(y_i-\hat{y}_i)^2}{N}}$		
%MARE (Percentage of Mean Absolute Relative Error)	$MAPE = \frac{\sum_{i=1}^{N}\left\lvert\frac{y_i-\hat{y}_i}{y_i}\right\rvert \times 100}{N}$		
%MdARE (Percentage of Median Absolute Relative Error)	$MdAPE = median\sum_{i=1}^{N}\left\lvert\frac{y_i-\hat{y}_i}{y_i}\right\rvert \times 100$		